LAWRENCE
LIVERMORE
NATIONAL
LABORATORY

LLNL-JRNL-684167

Review of even element super-heavy nuclei and search for element 120

S. Hofmann, S. Heinz, R. Mann, J. Maurer, G. Munzenberg, D. Ackermann, S. Antalic, W. Barth, H. G. Burkhard, L. Dahl, K. Eberhardt, R. Grzywacz, J. H. Hamilton, R. A. Henderson, J. M. Kenneally, B. Kindler, I. Kojouharov, R. Lang, B. Lommel, K. Miernik, D. Miller, K. J. Moody, K. Morita, K. Nishio, A. G. Popeko, J. B. Roberto, J. Runke, K. P. Rykaczewski, S. Saro, C. Scheidenberger, D. A. Shaughnessy, M. A. Stoyer, P. Thorle-Pospiech, K. Tinschert, N. Trautmann, J. Uusitalo, A. V. Yeremin

February 25, 2016

European Physical Journal A

Disclaimer

EPJ manuscript No.
(will be inserted by the editor)

Review of even element super-heavy nuclei and search for element 120

S. Hofmann[1,2,a], S. Heinz[1], R. Mann[1], J. Maurer[1], G. Münzenberg[1,3], D. Ackermann[1], S. Antalic[4], W. Barth[1], H.G. Burkhard[1], L. Dahl[1], K. Eberhardt[5], R. Grzywacz[6,7], J.H. Hamilton[8], R.A. Henderson[9], J.M. Kenneally[9], B. Kindler[1], I. Kojouharov[1], R. Lang[1], B. Lommel[1], K. Miernik[6,10], D. Miller[7], K.J. Moody[9], K. Morita[11], K. Nishio[12], A.G. Popeko[13], J.B. Roberto[6], J. Runke[1], K.P. Rykaczewski[6], S. Saro[4,b], C. Scheidenberger[1], H.J. Schött[1], D.A. Shaughnessy[9], M.A. Stoyer[9], P. Thörle-Pospiech[5], K. Tinschert[1], N. Trautmann[5], J. Uusitalo[14], and A.V. Yeremin[13]

[1] GSI Helmholtzzentrum für Schwerionenforschung, 64291 Darmstadt, Germany
[2] Institut für Physik, Goethe-Universität Frankfurt, 60438 Frankfurt, Germany
[3] Manipal Centre for Natural Sciences, Manipal University, Manipal 576104, Karnataka, India
[4] Department of Nuclear Physics and Biophysics, Comenius University, 84248 Bratislava, Slovakia
[5] Johannes Gutenberg-Universität Mainz, 55128 Mainz, Germany
[6] Oak Ridge National Laboratory, Oak Ridge, Tennessee 37831, USA
[7] University of Tennesee, Knoxville, TN 37996, USA
[8] Department of Physics and Astronomy, Vanderbuilt University, Nashville, Tennessee 37235, USA
[9] Lawrence Livermore National Laboratory, Livermore, California 94551, USA
[10] University of Warsaw, Warsaw, Poland
[11] RIKEN Nishina Center for Accelerator-Based Science, 2-1, Hirosawa, Wako, Saitama 351-0198, Japan
[12] Japan Atomic Energy Agency, Tokai, Ibaraki, 319-1195, Japan
[13] Joint Institute for Nuclear Research, 141980 Dubna, Russian Federation
[14] Department of Physics, University of Jyväskylä, 40351 Jyväskylä, Finland

Received: date / Revised version: date

This paper is dedicated to W. Greiner on the occasion of his 80th birthday

Abstract. The reaction ^{54}Cr + ^{248}Cm was studied at the velocity filter SHIP at GSI, Darmstadt, with the intention to study production and decay properties of isotopes of element 120. Three correlated signals were measured, which occurred within a period of 279 ms. The heights of the signals correspond with the expectations for a decay sequence starting with an isotope of element 120. However, a complete decay chain can not be established, since a signal from the implantation of the evaporation residue can not be identified unambiguously. Measured properties of the event chain are discussed in detail. The result is compared with theoretical predictions and with decay properties of even element super-heavy nuclei, which were compiled after a review of previously measured data. In the course of this review, a few tentatively assigned data could be corrected. New interpretations are given for results which could not be assigned definitely in previous studies. The discussion revealed that the cross-section for production of element 120 could be high enough so that a successful experiment seems possible with presently available techniques. However, a continuation of the experiment at SHIP for a necessary confirmation of the results obtained in a relatively short irradiation of five weeks is not possible. Therefore, we decided to publish the results of the measurement and of the review as they exist now. In the summary and outlook section we also present concepts for the continuation of research in the field of super-heavy nuclei.

PACS. 23.60.+e α decay – 25.70.Jj Fusion and fusion-fission reactions – 25.85.Ca Spontaneous fission – 27.90.+b A $\geq$ 220, super-heavy nuclei

1 Introduction, theoretical background, and status of experiments

Scientific attempts to synthesize new elements beyond uranium started in the middle of the 1930s, when the atomic model was established and the constituents of the atomic

[a] *Email:* S.Hofmann@gsi.de
[b] deceased in 2013

nucleus, protons and neutrons, were known. E. Fermi and E. Segré in Rome and O. Hahn, L. Meitner, and F.W. Straßmann in Berlin tried to use the nuclear reaction of neutron capture by uranium target nuclei and subsequent β^- decay for production of transuranium elements. Although most of the existing macroscopic quantities of transuranium elements up to einsteinium were produced later in nuclear reactors by this process, the discovery of Hahn and Straßmann [1] in 1938 was that uranium, more accurate the odd-mass isotope ^{235}U, breaks into two approximately equal parts after neutron capture. This new phenomenon of nuclear fission was described by Meitner and O.R. Frisch in 1939 using the charged liquid-drop model [2]. One year later, G.N. Flerov and K.A. Petrjak [3] detected that uranium, ^{238}U, decays spontaneously by fission from its ground-state.

The first new elements beyond uranium were synthesized during the years of the Second World War in laboratories in the US. These were the elements neptunium (Z = 93), plutonium (94), americium (95), and curium (96) (for details see e.g. G.T. Seaborg and W.D. Loveland [4]). In the years 1948−55 the elements berkelium (97), californium (98), einsteinium (99), fermium (100), and mendelevium (101) were also produced in the US. The production processes were fusion using a ^{4}He beam from the 60-inch cyclotron in Berkeley (^{242}Cm, ^{243}Bk, ^{245}Cf, ^{256}Md), slow neutron capture by ^{240}Pu produced from ^{239}Pu and subsequent β^- decay in a nuclear reactor (^{241}Am) or capture of fast neutrons from a reaction of ^{2}H with ^{9}Be by ^{238}U and subsequent β^- decay (^{239}Np), and rapid capture of 15 and 17 neutrons by ^{238}U in a thermonuclear explosion and subsequent β^- decays (^{253}Es, ^{255}Fm).

Chemical separation of these new elements was essential for the identification, as it was already for the discovery of nuclear fission, which was identified by the observation of barium in a chemically separated sample. In the region of heavy elements, these studies resulted in the concept of a second series of chemically similar elements, the actinides, starting at element 89, actinium, besides the known lanthanides, both having unfilled f-electron shells. In 1951 Seaborg and E.M. McMillan received the Nobel Prize in Chemistry, "for their discoveries in the chemistry of the transuranium elements".

Limits of existence of nuclei were estimated by J.A. Wheeler in 1955 [5,6]. Solely based on the charged liquid-drop model, the results seemed reasonable, "to look for nuclei with a well defined existence with masses perhaps two or more times heavier than the heaviest nucleus now known, ^{256}100". Whereas in [5] these nuclei were still named 'very heavy nuclei', the term 'superheavy nuclei', now usually abbreviated SHN, was used in [6] for the first time. Two years later, F.G. Werner and Wheeler published a paper with the title 'Superheavy Nuclei', in which the properties of these nuclei were estimated in more detail but still disregarding shell effects.

In addition, in this paper the authors discussed the problem of the binding of electrons in the strong electric field of such 'superheavy nuclei' considering the question that atoms having a charge higher than 137 units may exist only due to the finite size of the nucleus. This question was brought up by D.I. Blokhintsev in the discussion of Wheeler's contribution at the conference in Geneva in 1955 [6]. It is interesting to note that this subject and related vacuum polarization and electron-positron pair creation in strong electric fields became later a major topic of

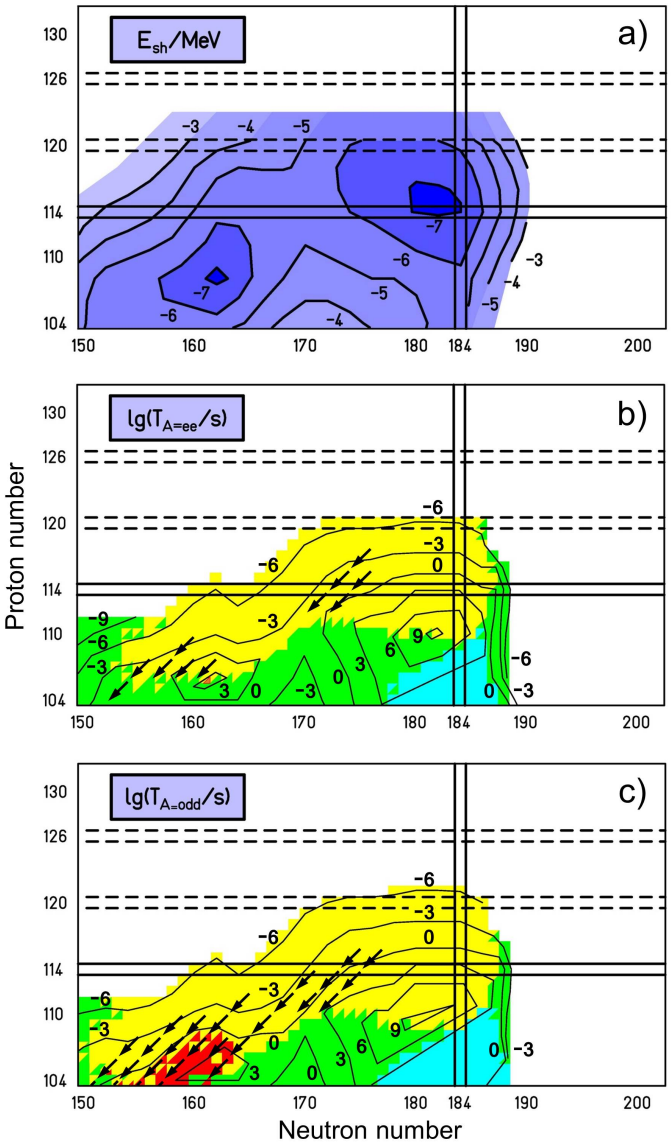

Fig. 1. Shell-correction energies in MeV taken from [7,8] (a) and dominating decay modes of even-even nuclei (b) and of even-odd nuclei (c). Using partial half-lives calculated in [7–9], the resulting dominating decay modes are plotted for α decay (yellow), β^+ decay or electron capture (red), β^- decay (blue), and SF (green) for even-even nuclei in (b) and for even-odd nuclei in (c). Arrows mark measured decay chains starting at the even element isotopes ^{264}Hs, ^{270}Ds, ^{268}Hs, ^{270}Hs, ^{294}118, and ^{292}Lv in (b) and at ^{263}Hs, ^{269}Ds, ^{271}Ds, ^{277}Cn, ^{271}Hs, ^{285}Fl, ^{291}Lv, and ^{293}Lv in (c). The α-decay chains end by SF in agreement with predictions.

theoretical studies and experimental work at GSI (Gesellschaft für Schwerionenforschung) in Darmstadt [10–12].

Although the charged liquid-drop model reproduces many collective properties of the nuclei very well, some known non-uniform structures demanded for a microscopic description. The increased binding energy of nuclei at the 'magic' proton or neutron numbers 2, 8, 20, 28, 50, and 82 is the most obvious example. For neutrons, N = 126 was also identified as a magic number. However, the highest stability was observed in the case of the 'doubly magic' nuclei with a closed shell for both protons and neutrons. Amongst other special properties, the doubly magic nuclei are spherical and resist deformation.

In 1948, the magic numbers were successfully explained by the nuclear shell model [13,14], and an extrapolation into the region of the next doubly magic nuclei beyond ^{208}Pb was thus undertaken. The numbers 126 for the protons, later changed to 114, and 184 for the neutrons were predicted to be the next spherical shell closures.

The perspectives offered by the nuclear shell model for production of SHN and the need for developing more powerful accelerators for their synthesis in heavy ion reactions was a main motivation for upgrading existing facilities or for founding new laboratories. In expectation of broad research fields the HILAC (Heavy Ion Linear Accelerator), later upgraded to the SuperHILAC, was built at LBNL (Lawrence Berkeley National Laboratory) in Berkeley in 1955, the U-300 and U-400 cyclotrons at FLNR (Flerov Laboratory of Nuclear Reactions) at JINR (Joint Institute for Nuclear Research) in Dubna in 1957 and 1978, respectively, the UNILAC (Universal Linear Accelerator) at GSI in 1969, and the RILAC (RIKEN variable-frequency Linear Accelerator) at the RIKEN Nishina Center in Saitama near Tokio in 1980.

Studies of the elements 100 to 106 were performed with the new cyclotron U-300 using fusion reactions with beams of ^{12}C to ^{22}Ne. In recognition of this early work in Dubna, element 105 is now officially named dubnium.

At approximately the same time, the experiments at the HILAC in Berkeley culminated in the synthesis of the new element 106. After careful investigation of discovery profiles by the International Unions of Pure and Applied Chemistry (IUPAC) and Physics (IUPAP), the names nobelium, lawrencium, and rutherfordium are now officially accepted for the elements 102, 103, and 104, respectively, as well as seaborgium for element 106.

In the middle of the 1960s, the concept of the macroscopic-microscopic (MM) model for calculating binding energies of nuclei also at large deformations was invented by V.M. Strutinsky [15]. In this model, the binding energy is calculated as sum of a predominating macroscopic part derived from the charged liquid-drop model of the nucleus and a microscopic part derived from the nuclear shell model. In this way more accurate values for the binding energy are obtained than in the cases of using only the liquid-drop model or the shell model.

Using this method a number of the measured phenomena could be naturally explained by considering the change of binding energy as function of deformation. In particular, it became possible to calculate the binding energy of a heavy fissioning nucleus at each point of the fission path and thus to determine the fission barrier.

The most important results which could be explained applying the Strutinsky method for calculation of the fission barrier are the fission isomers discovered by S.M. Polikanov *et al.* [16], which gain their stability from a second minimum in the fission barrier at large deformation, and the detection of the break of systematically long half-lives of N = 152 isotones at element 104 by Yu.Ts. Oganessian *et al.* [17] due to the disappearance of a second hump in the fission barrier.

Calculations using the MM model also revealed that the liquid-drop fission barrier decreases below 2 MeV for nuclei above fermium and vanishes completely for elements above 110. For these nuclei a fission barrier emerges only due to shell effects. The ground-state of these nuclei is formed by the configuration having the most negative shell correction energy (SCE) and thus highest stability. However, at increasing number of protons, the increasing Coulomb repulsion attributed to the liquid-drop part of the MM model results in a high fission probability already at small deformations. This is the reason why the second hump in the fission barrier vanishes at element 104 (see fig. 21 in [18]).

Calculations of ground-state SCE as function of deformation for heavy and super-heavy nuclei revealed a minimum (maximum in terms of stability) not only for spherical SHN at Z = 114 and N = 184, but also for deformed nuclei at Z = 108 and N = 162 [18]. For a wide range of heavy and super-heavy nuclei, SCE values of nuclei in the ground-state are plotted in fig. 1a. The values were taken from a calculation of A. Sobizcewski *et al.* [8]. The two minima, both having SCE values of −7 MeV, are clearly visible.

The shift of SHN with lowest SCE values to the region slightly above 114 and slightly below 184 is due to the low level density for the protons between 114 and 126 and for the neutrons between 164 and 184, see graphs 53 and 54 in [9]. The nuclei at Z = 108 and N = 162 gain their stability from relatively high level densities below gaps of single particle levels for these nucleon numbers at deformations characterized by the deformation parameters $\beta_2 \approx 0.22$, $\beta_4 \approx -0.07$ [8].

The maximum of SCE values between the two minima separates the region of heavy and super-heavy nuclei. Roughly, the borderline follows the line of constant mass number at A = 280. This definition of SHN is in agreement with definitions given in early calculations of the stability of SHN. However, it differs from the definition used by nuclear chemists nowadays, who define as super-heavy elements (SHE) the elements beyond the actinide series beginning with rutherfordium, element 104.

Problematic was the calculation of spontaneous fission (SF) half-lives of SHN. Predicted half-lives based on the Strutinsky model using various parameter sets differed by many orders of magnitude [18–27]. Some of the half-lives approached the age of the universe, and attempts have been made to discover naturally occurring SHN [28–30].

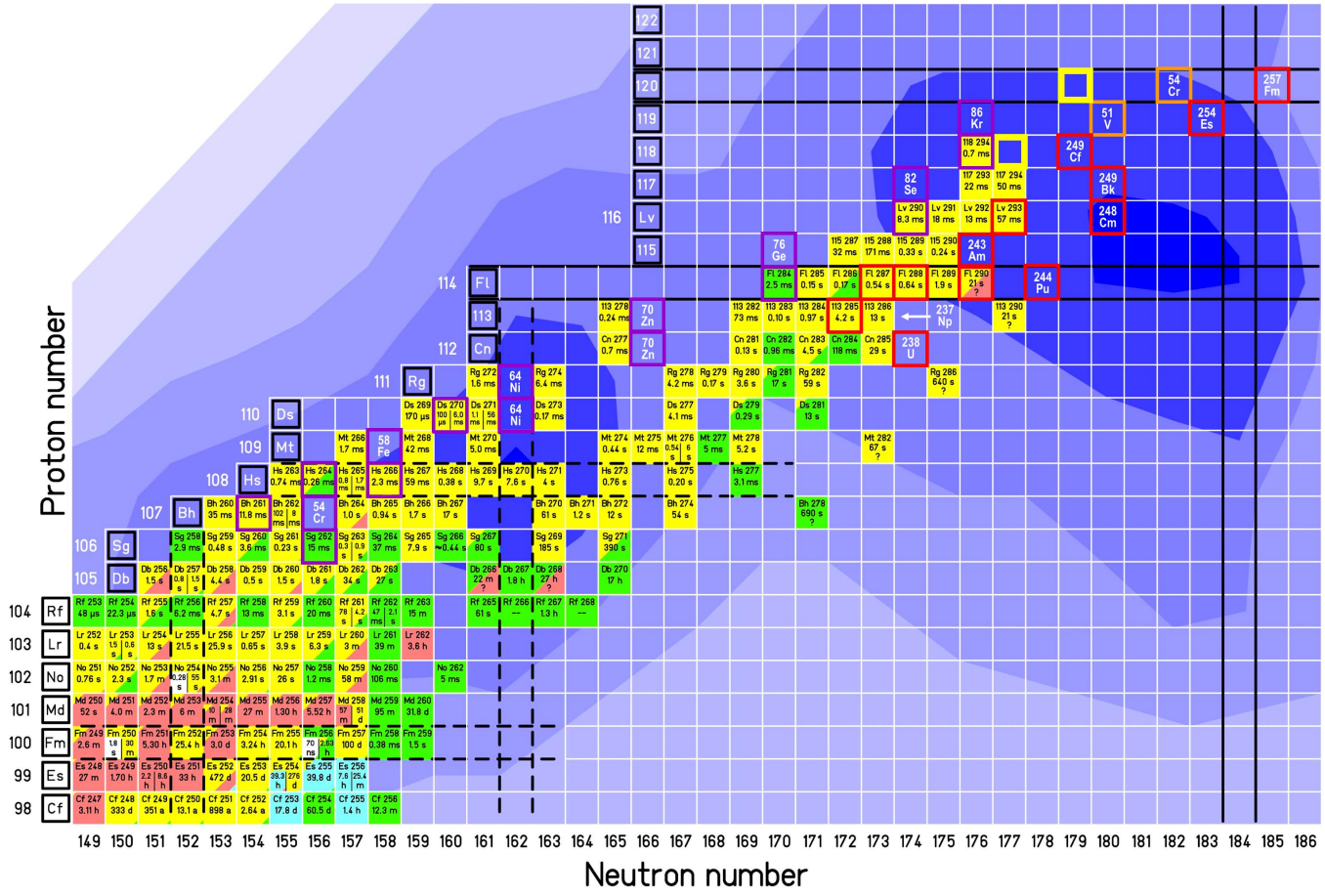

Fig. 2. Upper end of the chart of nuclei showing the presently (2016) known nuclei. For each known isotope the element name, mass number, and half-life are given. Colours are attributed to their decay mode: α decay yellow, β^+ or electron-capture decay red, β^- decay blue, SF green, and γ decaying isomers white. The relatively neutron-deficient isotopes of the elements up to proton number 113 were produced in cold fusion reactions based on ^{208}Pb and ^{209}Bi targets after evaporation of one or two neutrons from the CN (purple frames with isotope of the beam in white). Not yet studied or studied with negative results are the reactions using beams of ^{76}Ge, ^{82}Se, and ^{86}Kr. The more neutron-rich isotopes from element 112 to 118 were produced in reactions using a ^{48}Ca beam and targets of ^{238}U, ^{237}Np, ^{239}Pu, ^{240}Pu, ^{242}Pu, ^{244}Pu, ^{243}Am, ^{245}Cm, ^{248}Cm, ^{249}Bk, and ^{249}Cf. Red frames with the isotope of the target in white mark the CN. Not yet studied are reactions with the extremely difficult to produce targets of ^{254}Es and ^{257}Fm. Their CN are already in a region of decreasing shell-correction energy. Frames in orange mark the CN of reactions with a ^{248}Cm target and beams of ^{51}V (not yet studied) and ^{54}Cr (studied in this work). The expected residue after evaporation of three neutrons is ^{299}120 which α decays into ^{295}118, yellow frames. An attempt to re-interpret an event chain originally assigned to an α-decay chain starting at ^{289}Fl in [31] was made by assigning this chain to ^{290}Fl which decays by electron capture to ^{290}113, see sect. 4.7 and end of sect. 5.1.2. The magic numbers for protons at element 114 and 120 are emphasized. The bold dashed lines mark proton number 108 and neutron numbers 152 and 162. Nuclei with that number of protons or neutrons have increased stability; however, they are deformed contrary to the spherical super-heavy nuclei. At Z = 114 and N = 162 it is uncertain whether nuclei in that region are deformed or spherical. The background structure shows the calculated shell correction energy according to the macroscopic-microscopic model [7,8], see fig. 1a.

Although the corresponding discoveries were announced from time to time, none of them could be substantiated after more detailed inspection.

Even the location of the closed shells for protons and neutrons turned out to be model dependent. Self-consistent Hartree-Fock-Bogoliubov calculations and relativistic mean-field models [32–37] predict for spherical nuclei shells at Z = 114, 120, or 126 (indicated as dashed lines in fig. 1) and N = 172 or 184. The uncertainty in Z and N is due to the shell model the spin-orbit splitting resulting in the occurrence of subshells of low angular momentum between 114 and 126 for the protons and between 164 and 184 for the neutrons. For these very heavy nuclei the spin-orbit splitting is a function of the surface diffuseness which is difficult to determine. In particular, since some calculations even predict a lower density inside the nuclei resulting in a second, positive density gradient near the surface of the nucleus [38].

In parallel to progress in the discovery of new isotopes and elements in the region of heavy nuclei, the theoretical

models and computer programs could be improved due to advances of computer technology. Therefore, up to the heaviest known nuclei good agreement with experimental data for SF, α, β^-, and β^+ decay or electron capture (EC) is now obtained for even-even nuclei using the most advanced MM models [7–9]. The shortest half-lives which determine the decay mode are plotted in fig. 1b for even-even nuclei and in fig. 1c for even-odd nuclei. For the odd nuclei partial α and SF half-lives calculated in [8] were multiplied by a factor of 10 and 1000, respectively, thus making provisions for the odd particle hindrance factors. However, one has to keep in mind that, in particular, fission hindrance factors show a wide distribution from 10^1 to 10^5, which is mainly a result of the specific levels occupied by the odd nucleon [6,39].

For even-even nuclei in fig. 1b, the two regions of deformed heavy nuclei near N = 162 and spherical SHN merge and form a region of α emitters surrounded by spontaneously fissioning nuclei. Alpha decay becomes the dominant decay mode beyond Z = 110 with continuously decreasing half-lives. For nuclei at N = 184 and Z < 110 half-lives are determined by β^- decay. For even-odd nuclei, fig. 1c, the island character of α emitters disappears and for nuclei with neutron numbers 150 to 160 α decay prevails down to element 104 and beyond.

Longest total half-lives do not occur for nuclei having the most negative SCE values. Due to the short partial α half-lives there, the longest half-lives of SHN are predicted for nuclei near element 110 and neutron number 182.

The interesting question arises, if and to which extent, uncertainties related to the location of proton and neutron shell closures change the half-lives of SHN. Partial α and β half-lives are only insignificantly modified by shell effects because their decay process occurs between neighboring nuclei. This is different for fission half-lives which are primarily determined by shell effects. However, the uncertainty related to the location of nuclei with the strongest shell-effects, and thus longest partial SF half-life at Z = 114, 120, or 126 and N = 172 or 184, is irrelevant concerning the longest 'total' half-life of SHN. The decays of all of these SHN are dominated by α decay. Alpha-decay half-lives are only modified by a factor of up to approximately 100 compared to the calculations used in fig. 1, if the double shell closure is not located at Z = 114 and N = 184. Only if shell effects are as strong as in the double magic ^{208}Pb, the half-lives could become significantly shorter for nuclei above the shell closure and longer for the nuclei below.

The line of reasoning is, however, different concerning the production cross-section. The survival probability of the compound nucleus (CN) formed in a heavy ion fusion reaction is mainly determined by the fission barrier. Therefore, for reliably estimating the production cross-section, the knowledge of the location and strength of minimal negative SCE is highly important. However, it may also turn out that shell effects in the region of SHN are distributed across a number of subshell closures, *e.g.* for the proton numbers 114, 120, and 126. In that case a wider region of less deep shell-correction energy would exist with corresponding modification of stability and production yield of SHN.

Alternatively to fusion-evaporation reactions, the possibility of multi-nucleon transfer reactions using the heaviest feasible beams and targets was considered. Therefore, acceleration of beams as heavy as uranium was included in the design goals of the UNILAC at GSI. However, as soon as relevant experiments could be performed, it turned out that the most successful methods for the laboratory synthesis of SHN are fusion-evaporation reactions using heavy-element targets, recoil-separation techniques, and the identification of the nuclei by generic ties to known daughter decays after implantation into position-sensitive detectors [40–42].

The newly developed detection methods extended the range of measurable half-lives considerably. The lower half-life limit of about 1 μs is determined by the flight time through the separator. Long half-lives are measurable up to about one day. There, the limitation is given by the rate of implanted reaction products and background considerations. The position-sensitive Si detectors are capable of measuring all radioactive decays based on particle emission like proton radioactivity, α and β decay, and SF. Additional Ge detectors surrounding the Si detectors measure coincident or delayed coincident γ rays, X rays or high energy β particles.

A further extension of the measuring possibilities was achieved with γ ray, X ray, or particle detectors mounted around the target. If these detectors are operated in delayed coincidence with signals from the implantation of reaction products and their radioactive decay in the focal plane of the separator, the sensitivity of 'in-beam' spectroscopy is significantly improved. This so called recoil decay tagging (RDT) method was first applied in a study of the heavy ion radiative capture mechanism, a cold fusion process at excitation energies of the CN below the separation energy of protons and neutrons so that the excitation energy can be emitted only by γ rays. The successfully studied reaction was $^{90}\mathrm{Zr} + {}^{90}\mathrm{Zr} \rightarrow {}^{180}\mathrm{Hg}$ [43]. Meanwhile the method has become a standard tool in nuclear in-beam spectroscopy, and it has become known as the RDT technique.

Detailed descriptions of the set-ups of the physics experiments used for the investigation of SHN are given in review articles [42,44–48]. Cold and hot fusion reactions based on targets of lead or bismuth and isotopes of actinides, respectively, were used for the synthesis of heavy and super-heavy nuclei. These experiments resulted in the identification of the new elements 107 to 112 at the vacuum velocity filter SHIP (Separator for Heavy Ion reaction Products) at GSI [42], in the confirmation of these data and in the production of a new isotope of element 113 at GARIS (Gas-filled Recoil Ion Separator) at RIKEN [48]. New neutron-rich isotopes of element 112 and the new elements from 113 to 118 were produced at DGFRS (Dubna Gas-Filled Recoil Separator) at FLNR [47]. Isotopes which are presently known in the region of heavy and super-heavy nuclei are shown in fig. 2.

Despite the synthesis of nuclei as heavy as ^{294}118, the extension of the island in proton and neutron numbers and also the locations of the centers of highest stability resulting in highest production cross-sections and that of longest half-lives is not yet explored. The reasons are experimental constraints like availability of targets, limited beam intensities and consequently long measuring times at cross-section levels of picobarn and below.

A key role in answering some of the open questions plays the synthesis of isotopes of element 120. However, recent attempts using fusion reactions with targets of ^{244}Pu [49], ^{238}U [50] were negative or, as in the case of ^{249}Cf [51], the data are not yet completely analyzed.

In an attempt to produce an isotope of element 120, we investigated the reaction ^{54}Cr + ^{248}Cm → ^{302}120* at SHIP. This reaction is more asymmetric than the reactions ^{64}Ni + ^{238}U and ^{58}Fe + ^{244}Pu and thus less Coulomb repulsion exists in the entrance channel. Although the reaction ^{50}Ti + ^{249}Cf is even more asymmetric, in our choice we expect to profit from being three neutrons nearer to the N = 184 shell closure. To date, the measured cross-sections were always higher when more neutron rich projectile and/or target isotopes were used. In our experiment, we planned to reach a cross-section limit of 100 fb for which a beam time of 140 days was requested.

Technical arguments are an additional reason for using a ^{248}Cm target. This isotope is an α emitter with a long half-life of 3.4×10^5 years, and it has a low SF branching of 8 %. The resulting specific activity is low so that target wheels can be produced and handled without using special manipulators and heavy radiation shielding. Most important, the isotope ^{248}Cm can be produced in nuclear reactors in larger quantities. The current inventory at ORNL (Oak Ridge National Laboratory) is 2,500 mg [52]. Due to the long half-life such a target does not decay much even during long-lasting experiments.

Safe operation under the experimental conditions was tested in a preparatory experiment in 2010 [53]. In the reaction ^{48}Ca + ^{248}Cm → ^{296}Lv* previous results on the decay of ^{293}Lv and ^{292}Lv were confirmed and, in one case, new decay data of the daughter nuclei of ^{293}Lv were tentatively assigned to isomeric transitions (a new interpretation of this tentatively made assignment is given in sect. 4.4).

In this paper, we present and discuss correlated signals observed in the reaction ^{54}Cr + ^{248}Cm during a first part of 38 days of the experiment. The energies of the signals are in agreement with calculated values of the α energies of ^{299}120 and its daughter isotope ^{295}118 [9,54,55]. The third signal agrees with the previously measured α energy and lifetime of the granddaughter ^{291}Lv [56]. However, the lifetimes of the two nuclei starting the decay chain, differ from expectations.

An observed SF event which could be the termination of the chain, deviates from confirmed decays of ^{287}Fl and ^{283}Cn [57]. Therefore, we critically reviewed all published information on even elements beyond darmstadtium measured in reactions with actinide targets so far, in order to get additional arguments for an assignment from the systematics of experimental data. Also attempts were made interpreting measured and published data which could not yet be confirmed but could possibly be interpreted on the basis of more experimental data now available.

A statistical analysis of the data trying to explain the event chain observed in the ^{54}Cr + ^{248}Cm irradiation as a random event revealed that this probability is very low. The most reasonable procedure for proving or disproving the result under these circumstances would be the continuation of the experiment. However, beam time is presently not available, and it is uncertain if and when SHN experiments at SHIP can be performed again in the future. Therefore, we use this opportunity to present details of the experiment and the analysis, which is usually not possible in shorter publications. This way we best illustrate the advantages of the experimental method and its limitation.

For those reasons, we are convinced that publication of the data as it was measured in 2011 is most reasonable, together with a presentation of the results of the review of existing data. In the summary and outlook section, we also present concepts and perspectives for the continuation of research in the field of SHN.

2 Experimental method

The experiment was performed at the UNILAC of GSI. The beam of ^{54}Cr ions was extracted from the ECR ion source with charge state of 8^+. The consumption of ^{54}Cr having an enrichment of 99.8 % was 3.8 g during an operation time of 38 days, which corresponds to a consumption rate of 4.2 mg/h.

The targets were prepared from isotopically enriched curium having an enrichment of 96.85 % of ^{248}Cm. Impurities of lighter curium isotopes were 0.015 % of ^{247}Cm, 3.10 % of ^{246}Cm, 0.031 % of ^{245}Cm, and 0.0007 % of ^{244}Cm. Preparation of the targets consisting of a layer of $^{248}CmO_{1.75}$ (mixture of $^{248}CmO_2$ and $^{248}Cm_2O_3$) on a titanium-backing foil was described in detail in our publication on the synthesis of livermorium isotopes produced in the reaction ^{48}Ca + ^{248}Cm [53]. There, also details of the target control, the separation of the reaction products by SHIP, the detector set-up, the electronics, the measured ranges for detection of α and SF decay energies, the settings of the discriminator levels, and the analysis procedure are given. For an easier understanding of the following discussion, we show the detector system with the relevant detectors and detector numbers emphasized in fig. 3.

As in our previous experiment, the last dipole magnet of SHIP was adjusted to an angle of –4 degrees relative to the beam direction. An asymmetric setting of the first quadrupole triplet of SHIP was applied, which was calculated using a Monte Carlo method [58]. This setting resulted in a calculated overall efficiency of 22 % for evaporation residues (ER) from 3n and 4n evaporation channels at a target thickness of 0.512 mg/cm^2 of $^{248}CmO_{1.75}$ and of 27 % at 0.417 mg/cm^2. The different thicknesses of $^{248}CmO_{1.75}$ and of the ^{248}Cm fraction are given in table 1. The calculation of the efficiency considered a Gaussian

Table 1. Experiment parameters of the study of the reaction ^{54}Cr + ^{248}Cm at the velocity filter SHIP in 2011. The beam pulses from the accelerator UNILAC had a width of 5.2 ms at a repetition frequency of 20 Hz. The notation pnA stands for particle nA (1 pnA = 6.24×10^9 particles/s). Parts 1 and 2 were measurements with the same wheel, however, at higher beam intensity in part 2. Part 3 shows the data measured with the second wheel with thinner targets.

	Part 1	Part 2	Part 3
Target wheel number	1	1	2
Dates in 2011	24.04.–13.05.	13.05.–24.05.	26.05.–01.06.
Calendar days	19	11	8
Beam on target/day	17	10	7
Maximum current/pnA	500	600	500
Mean current/pnA	371	445	318
Beam dose/10^{18}	3.4	2.4	1.2
d(Ti-backing)/(mg cm^2)	1.05	1.05	1.06
d(^{248}CmO$_{1.75}$)/(mg cm^2)	0.512	0.512	0.417
d(^{248}Cm)/(mg cm^2)	0.458	0.458	0.375
Beam energy/MeV	325.9	325.9	325.0
E_{54Cr}/MeV$^{(a)}$	307.8–305.1–302.5	307.7–305.1–302.5	306.6–304.5–302.4
E*/MeV$^{(a)}$	44.0–41.9–39.7	44.0–41.9–39.7	43.1–41.4–39.6
E_{ER}/MeV$^{(a)}$ in target	54.5–54.1–53.6	54.5–54.1–53.6	54.3–53.9–53.6
E_{ER}/MeV$^{(a,b)}$ before stop detector	41.6–45.3–49.3	41.6–45.3–49.3	43.5–46.3–49.3
R_{ER}/μm$^{(a,c)}$	4.6–5.1–5.6	4.6–5.1–5.6	4.8–5.1–5.5
Total ER efficiency/%	22	22	27
Cross-section limit/pb$^{(d)}$	1.2	1.7	3.4

$^{(a)}$ Values are given for reactions at the beginning, at the center and at the end of the curium-oxide layer.
$^{(b)}$ Calculated kinetic energy of ER's before implantation into the Si stop detector.
$^{(c)}$ Range of ER's stopped in the Si detector.
$^{(d)}$ Given as limit is the one event cross-section. The one event cross-section from all three parts is $(0.58^{+1.34}_{-0.48})$ pb.

shaped excitation function having an assumed full width at half maximum (FWHM) of 10 MeV and scattering of the ERs in the target itself, in the charge equilibration foil, and the foils of the time-of-flight (TOF) detectors behind SHIP. Although the transmission is less using thicker targets, the losses are compensated by the higher amount of target nuclei available. Due to this interplay the yield for separation of fusion products reaches saturation at about 0.400 mg/cm^2 target thickness.

In the present experiment the data acquisition was augmented with digital pulse processing [59,60]. The energy pre-amplifier signals from the 16 strips of the stop detector and from the 28 segments of the box detector were independently analyzed with a sampling rate of 100 MHz. A 12 bit conversion allowed for an energy measurement between 1 and 30 MeV. Higher energy signals were registered as saturated events. The energy range from 0.16 to 16 MeV and from 4 to 320 MeV was covered in two branches by the analog electronics.

Vertical position signals from the stop detector were not yet integrated in the digital system. However, included were the signals from the veto detector, the TOF measurement, and the information on the on-off status of the beam. Due to the relatively low rates of interesting decay chains and background events, cross-correlation of the signals from the analogue electronics and the digital system was made with an occasional readout of specific events or event sequences measured in both systems.

The digital signal processing technique enabled detection of subsequent events following each other as prompt as ≈100 ns. An intelligent front-end pre-selection of single pulses was performed by delay-line shaping so that in the case of single events only time and amplitude were accumulated, similar as in the parallel analogue electronic circuit. Only in the case of pile-up were the complete pulse shapes registered. As a result, the amount of data was small, amounting to only 0.40 TBytes for all events stored from the digital system (it would have been 47 TBytes without the front-end signal processing) and another 0.10 TBytes for the events from the analogue electronics with conventional ADCs.

During the previous irradiation of the targets with ^{48}Ca, we observed a small rip in five of the eight target segments mounted on the first wheel. The present irradiation plan took into account this circumstance. In a first part of the experiment, this wheel was irradiated again; however, with moderate intensity. After a second wheel was prepared, the beam intensity was increased. Maximum values of 0.6 $p\mu$A (1 $p\mu$A = 6.24×10^{12} particles/s) were reached. Eventually, in a third part of 8 days of the experiment, the new wheel was irradiated again with moderate intensity. In this part the targets were conditioned for further use in a continuation experiment. No rips were

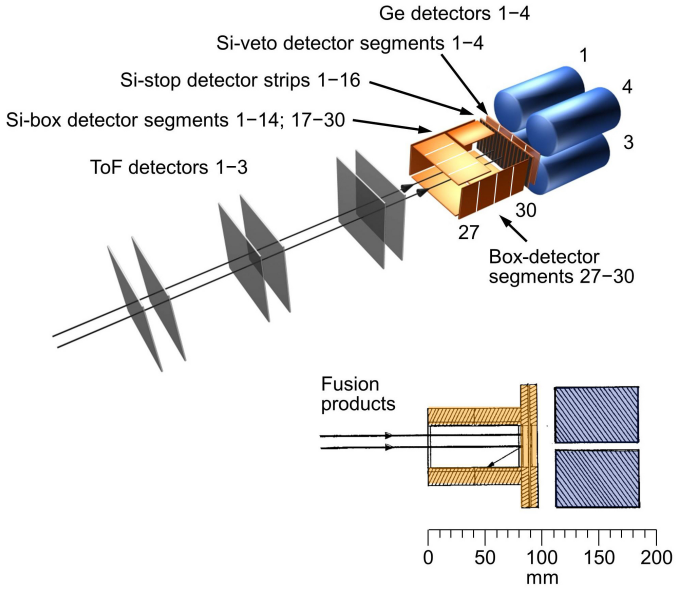

Fig. 3. Detector system. Emphasized are detector strip or segment numbers, which are relevant for the description of the present measurements. To reduce scattering in the carbon foils of the TOF detectors, in each of them the second foil was replaced by a grid of thin wires as described in [53]. For the same reason, reduction of scattering, only two of the three TOF detectors were used. From the beginning up to May 12 these were detectors 2 and 3. From then up to the end of the experiment foil 2 had to be replaced by foil 1 due to failure. The TOF detectors are mounted at distances of 780, 425 and 245 mm in front of the stop detector, in each case measured from the center between carbon foil and grid.

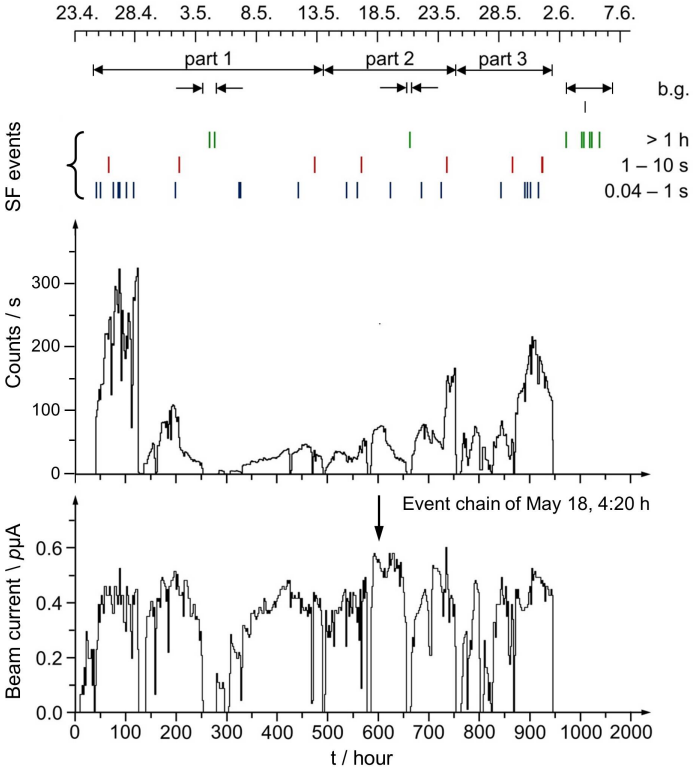

Fig. 4. Beam current (lower part, given is the average value in bins of 2 h) and rate of target like nuclei in the stop detector within an energy window from 18 to 40 MeV (middle part) plotted as function of the beam time. See text for an explanation of the measured SF events shown on top of the figure. Two longer periods during and one after the irradiations were used for background measurements. These periods are shown in the row marked 'b.g.' in the upper part of the figure. The time of the occurrence of the three events chain on May 18th is marked in the lower part.

observed in the targets of the second wheel after irradiation. Target parameters, beam currents, energies, beam doses, and other relevant parameters of the experiment are listed in table 1 separately for the three parts of the experiment.

The beam energy was chosen on the basis of excitation functions measured for reactions with ^{48}Ca beams and various actinide targets at FLNR [57]. There, maximum cross-sections were measured slightly below excitation energies (E*) of 40 MeV for 3n evaporation channels and slightly above 40 MeV for 4n channels. The experimental data are well in agreement with calculations which predicted also excitation functions for the reaction ^{54}Cr + ^{248}Cm [61]. Maximum cross-section values were calculated at 39 and 43 MeV for the 3n and 4n channel, respectively. In our experiment we chose beam energies so that E* covered a range from 44 to 40 MeV for reactions at the beginning and at the end of the target, respectively. For details see table 1.

The beam current on the target is plotted as function of time in the lower part of fig. 4. The irradiations started on April 23, 2011 at 9:00 h and the data acquisition on April 24 at 12:00 h. The irradiations ended on June 1 at 10:00 h. After the irradiation a period of four days ending at June 6 was added to measure the decays of detector implanted nuclei. The irradiations were interrupted five times by intervals necessary for the refilling of chromium in the oven of the electron-cyclotron resonance (ECR) ion source, and at various other short times for the alignment of the beam, optical target control, and detector calibration, amounting to a total of four days. During the net irradiation time of 34 days, a beam dose of 7.0×10^{18} was collected.

The beam current is compared with the rate of scattered target like nuclei having the same velocity as the expected ER of element 120, as shown in the middle part of fig. 4. These nuclei traverse through SHIP as background resulting in events with signal amplitudes between 18 and 40 MeV in the stop detector. The higher rate relative to the beam current at the beginning and two times close to the end of the beam time, is due to contaminations of higher energy beam particles. These contaminations, having energies up to 330 MeV instead of 326 MeV, were detected by the measurement of electrons which are pro-

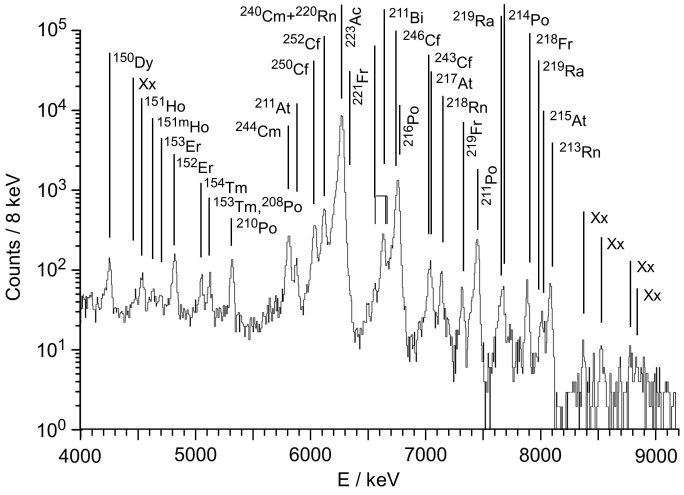

Fig. 5. Alpha singles spectrum taken during the beam-off periods. The spectrum shows all events occurring during the 14.8-ms pauses between the beam pulses and during the irradiation period of 25 days from May 5 to 30. Strip numbers 5, 9, 13 and 15 are not included, see text for details. The assignment of lines marked by 'Xx' as element symbol is still uncertain. The energy scale is shifted by a mean value of 40 keV for compensating the fraction of the recoil energies contributing to the height of the detector signals. In that case the scale corresponds to the α energies.

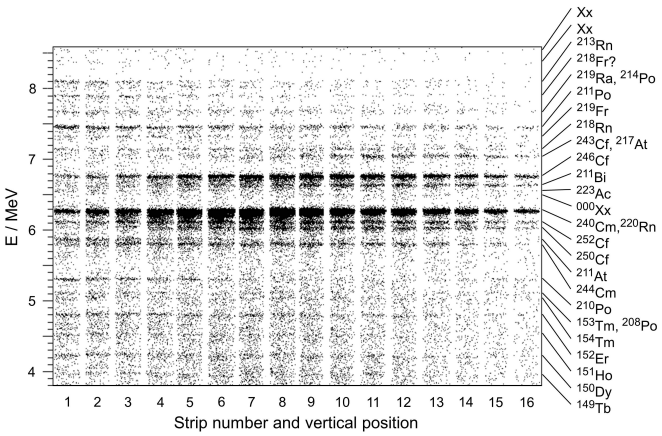

Fig. 7. Energy-position scatter plot of events in the beam pauses taken during 25 days beginning May 5. The abscissa shows for each of the 16 detector strips the vertical position ranging from 0 mm at the bottom to 35 mm at the top of the strip. The assignment of lines marked by '^{000}Xx' is still uncertain. Note that some α lines are focused more to the left side, some more to the center and some more to the right side in the focal plane. This distribution is a consequence of the charge and momentum dispersion arising from the last dipole magnet of SHIP. It indicates that the nuclei are produced in different reactions.

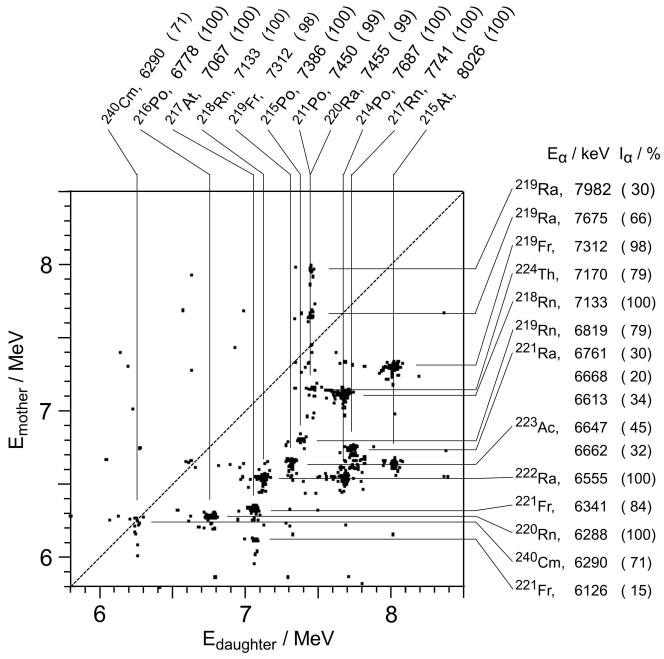

Fig. 6. Energies of mother-daughter delayed coincidences of events during the beam pauses within time and position windows of 1 s and $\pm$1mm, respectively. Given literature values of α energies and intensities were taken from [63]. The spectrum includes data measured during 25 days beginning May 5. Strip numbers 5, 9, 13 and 15 are not included, see text for details.

duced with beam velocity in collisions with the atoms of the residual gas [62]. The portion of higher energy was about 50 % in the worst case. The higher rate of target-like nuclei unfortunately also results in an increased background rate of α emitters and of SF events, see fig. 4. Details will be presented in the following section.

3 Results

3.1 Assignment of background events

A total spectrum of α emitters implanted into the stop detector is shown in fig. 5. The spectrum shows the projection of the raw data on the energy axis, which resulted in the best energy resolution. Strip numbers 5, 9, 13 and 15 are not included. For them a position dependent energy calibration was needed, which slightly reduces the energy resolution. The result obtained for all strips is shown in fig. 7.

The two most intensive lines were assigned to the α decays of ^{240}Cm (E$_\alpha$ = 6319 keV, T$_{1/2}$ = 27 d) and ^{246}Cf (6780 keV, 35.7 h). These nuclei are produced in inelastic nucleon-transfer reactions and subsequent neutron evaporation of the heavy reaction fragment. The relative intensity of these two and also of some other background α emitters was different during the periods with the contamination of higher energy beam particles. Therefore, the first period of the experiment up to May 5 is not included in the spectra.

Other isotopes of curium and californium that are presumably also produced were not observed during the irradiations due to long half-lives or small alpha-branching ratios. For the same reasons, isotopes of elements from protactinium to americium are not visible. However, some of these isotopes could be observed in spectra during longer beam-off intervals and in the four days of background measurement after the irradiations. Not observed in this experiment was the 11.65-MeV α decay of the 45-s isomer in ^{212}Po, which, however, was measured as a relatively strong line in the ^{48}Ca + ^{248}Cm experiment [53].

Most of the lines appearing with relatively weak intensity originate from isotopes of elements between lead and protactinium. The assignment of the peaks is based on mother-daughter correlations using reasonable position and time windows. An example of a two-dimensional mother-daughter correlation plot is shown in fig. 6.

The data analysis revealed production also of heavier nuclei. Clearly, α decays of ^{248}Cf (6319 keV, 333 d), ^{250}Cf (6056 keV, 13 y), ^{253}Es (6681 keV, 20.5 d), and ^{252}Fm (7070 keV, 25 h) were observed. The observation of these heavy nuclei is of interest with respect to the fusion path initiated by transfer of protons from the projectile to the target [45]. A detailed discussion of the production of these nuclei will be subject of a separate paper.

Also measured were α lines from N = 84 to 86 isotones of elements between dysprosium and ytterbium. These activities are produced in fusion reactions with a known target contamination of palladium, as discussed in our previous paper [53].

The distribution of the α activities in the focal plane is shown in fig. 7. We note that background lines with highest intensity are located in the left two-thirds of the stop detector, strip numbers 1 to 12. In the right third, especially in the most right detector strip number 16, the background of α decays during beam pauses is weakest.

Observed SF events characterized by energies greater than 100 MeV, are shown as function of time in the three rows on top of fig. 4. The events are subdivided in three groups according to different ranges of the lifetime. In the lowest row, signals are plotted which were measured in anti-coincidence to the TOF detectors and which were correlated to implanted nuclei. The distribution of these nuclei in the energy-TOF spectrum overlaps with the region of target-like nuclei. This and their lifetimes in the range from 40 μs to 1 s identifies these nuclei as fission isomers located in the chart of nuclei between neptunium and berkelium, one to eleven neutrons less than the target ^{248}Cm. The assignment is supported by the higher rate measured during the periods of contributions of higher beam energy at the beginning and at the end of the irradiations.

The middle row shows SF events occurring during the beam pauses, which, however, were correlated to implanted nuclei within a time range of 1 to 10 s. This group is tentatively assigned to nuclei above curium produced in inelastic reactions. Also in this case, the energy-TOF values of the implanted nuclei overlap with the region of target-like nuclei. A shift to higher energy and thus mass number is not observed due to insufficient resolution of the energy-TOF measurement. An additional study taking advantage of different velocity settings of SHIP could be performed in order to clarify if, *e.g.*, ^{252}No ($T_{1/2}$ = 2.3 s, b_{SF} = 27 %) is produced in this way.

Finally, the third group shows SF events with lifetimes longer than hours, which were measured during longer beam-off intervals on May 4 and 20 and after the irradiations. Except the energy condition of 100 MeV no other conditions are applied for these events. Unfortunately, the data taking and thus the measurement of the decay time of these long living nuclei could not be extended due to a follow up experiment. Therefore, assignments of these long living SF events based on measurements of the decay-time cannot be made.

However, an estimate shows that a fraction of the events could be due to elastically scattered target nuclei. It should be noted that SF events with such long lifetimes cannot be correlated to the corresponding ER due to the background conditions during beam-on intervals. Different, however, are the conditions in the case of rare α-decay chains ending by SF. Then, at SHIP, correlation times of up to days are possible, if the SF event occurs during a beam pause. In our experiment, the rate of such SF events is only about 1 per day for the whole detector and 0.002 per day per logic pixel having a size of 5×1 mm^2.

3.2 Observation of a 279-ms event chain in the energy range from 13.1 to 10.6 MeV

Already, in an early stage of the analysis, we found three correlated signals with energies expected for the α decay of an isotope of element 120. In particular, the energy and lifetime of the third signal is in perfect agreement with the known decay data of ^{291}Lv, which would be the granddaughter of ^{299}120 produced in a 3n evaporation channel. The energies of the first two signals are in agreement with predictions of the MM models for α decays of ^{299}120 and ^{295}118 [9,54,55].

The assignment of the three signals to an α-decay chain would be corroborated, if an initiating implanted ER could be found. However, the search for such an additional event was unsatisfactory, see sect. 3.2.4. On the other hand, an estimate of the probability that the event chain occurred by chance revealed a value far below one per million, see sect. 3.3. In the following we will present the parameters of the event chain in detail. The calculation of the chance probability and a comparison with known experimental data follows. Finally, the measured data are discussed within the framework of theoretical models.

The event chain was measured on May 18, 2011 at 4:20 h. At this time, the beam intensity was highest with maximum values of 0.6 $p\mu$A. However, the background rate of target-like nuclei within the energy window from 18 to 40 MeV was on the expected level of about 100 Hz at a total event rate of 200 Hz of all signals from the silicon detectors above the trigger level at 160 keV. During this period no admixture of unwanted beam energies was observed, see fig. 4. All three events were measured at

Table 2. Parameters of events of the chain $\alpha 1$, $\alpha 2$, and $\alpha 3$ measured in strip 16 of the stop detector on May 18, 2011, at 4:20 h. All neighboring events are also given. The events marked ER1, ER2, and ER3 and those marked SF1, SF2, and SF3 have parameters expected for implanted ER's or SF events occurring at the same position in strip 16. See text for further explanation. With $t_0 = 2{,}554\times10^9$ μs, column 2 shows the time when the events occurred, relative to the start of the clock on April 18 at 14:51 h. The time relative to event $\alpha 1$ is given in column 3. The time in column 2 modulo 20,000 μs gives the time during the 20 ms beam period with the beam-on phase from 0.3 to 5.5 ms. The letters N (north) and S (south) in column 5 identify the detectors for elastically scattered projectiles mounted with angles of ±30° relative to the beam direction.

Events	$t-t_0$ /μs	t_{rel}	E /MeV	strip or box no.	$y^{(a)}_{top}$ /mm	TOF /channel	remarks
ER3	134,285,246	–16.9 s	31.2	16	26.7	1077	TOF-1 and TOF-2
	...						847 events skipped
ER2	137,002,837	–14.2 s	28.9	16	22.1	1059	TOF-1 and TOF-2
	...						2639 events skipped
ER1	145,865,041	–5.4 s	26.0	16	22.6	1053	TOF-1 and TOF-2
	...						1568 events skipped
	151,205,247	–17.617 ms	23.6	9	5.9	1025	TOF-1 and TOF-2
	151,220,406	–2.458 ms	26.6	13	13.7	1045	TOF-1 and TOF-2
	151,220,600	–2.264 ms	2.288	11	box	937	TOF-1 and TOF-2
$\alpha 1$	**151,222,864**	**0 μs**	**13.140±0.030**	**16**	**22.8**	**–**	**no TOF, no VETO**
	151,223,417	0.553 ms	53	S	–	–	scattered projectile at target
	151,224,556	1.692 ms	3.116	7	9.7		TOF-1
	151,240,831	17.967 ms	6.867	15	27.6		no TOF
	...						63 events skipped
	151,464,763	241.899 ms	0.698	4	26.7	910	TOF-1 and TOF-2
	151,464,788	241.924 ms	302	S			scattered projectile at target
	151,464,882	242.018 ms	210	N			scattered projectile at target
$\alpha 2$	**151,483,933**	**261.069 ms**	**11.814±0.040**[b]	**16**	**25.4**	**–**	**no TOF, no VETO**
	151,484,535	261.671 ms	6.476	11	5.3	1079	TOF-1 and TOF-2
	151,500,607	277743 ms	108	S			scattered projectile at target
	151,500,785	277921 ms	2.107	14	11.1		TOF-1
	151,501,373	278509 ms	3.477	14	17.3	903	TOF-1 and TOF-2
$\alpha 3$	**151,502,311**	**279.447 ms**	**10.698±0.030**[c]	**16**	**24.4**	**–**	**no TOF, no VETO**
	151,502,411	279.547 ms	28.8	4	30.2	1079	TOF-1 and TOF-2
	151,504,372	281.508 ms	25.6	7	17.8	1054	TOF-1 and TOF-2
	151,505,011	282.147 ms	26.7	10	9.2	1064	TOF-1 and TOF-2
	...						5835 events skipped
($\alpha 4$)[d]	171,382,305	20.159 s	0.353	16	24.3	–	no TOF, no VETO, no BOX
	...						11815 events skipped
	213,761,184	62.538 s	1.985	16	24.9	–	no TOF, no VETO, no BOX
	...						6,057 events skipped
	235,303,306	84.080 s	3.994	16	26.3	–	no TOF, no VETO, no BOX
	...						183,508 events skipped
SF1	**872,661,757**	**12.02 min**	**158.6**	**16**	**24.7**	**–**	**no TOF, no VETO**
	...						24,454,780 events skipped
SF2	92,221,381,053	25.6 h	190.6	16	26.2	–	no TOF, no VETO
	...						2,835,893 events skipped
SF3	101,408,563,581	28.1 h	118.4	16	22.9	–	no TOF, no VETO

[a] The vertical position y_{top} ranges from 0 mm at the bottom to 32 mm at the top of the strip. The mean value of the positions of the events $\alpha 1$, $\alpha 2$, and $\alpha 3$ is 24.2 mm.
[b] Sum of energies 4.936 MeV and 6.878 MeV measured in stop-detector strip 16 and box-detector segment 27, respectively.
[c] The α particle was followed by a 998-keV signal in Ge-detector number 4 at $\Delta t = 265$ ns at a width of the prompt peak of $\sigma = \pm 47$ ns.
[d] Possible escape event $\alpha 4$, see discussion at the end of sect. 5.2.

times when the rips in the targets were not hit by the beam. The cycling of the rips through the beam results in a locally increased background which, however, does only slightly increase the average background rate. It was not subtracted from the average rates during beam pulse which are used for calculation of the chance probabilities.

The event chain occurred in strip number 16 at a vertical distance of 24.2 mm from the bottom. In strip 16 the background rate of signals greater than 3 MeV is lowest in the singles spectrum (fig. 8c), however, it is highest in the anti-coincidence spectrum (fig. 8b). Figure 8 and the composition of the background is described in sect. 3.2.1. The three signals of the chain were found within a vertical range of ±1.3 mm. For the energies we determined values of (13.14 ± 0.03), (11.81 ± 0.04), and (10.70 ± 0.03) MeV. The time between the first and the second event was 261 ms and between the second and third event 18.4 ms. All signals appeared during the 5.2-ms beam-on periods, however, in anti-coincidence to the two TOF detectors and the veto detector. Energies with error bars, positions, time, and time differences are listed in table 2 in the rows marked α1, α2, and α3. The measured cross-section of the event chain considering all three parts of the experiment is $(0.58^{+1.34}_{-0.48})$ pb. The given error bars represent the statistical uncertainties for one event at a confidence level of 68 % [64]. An estimate of systematic uncertainties resulted in another factor of two, which includes uncertainties of target thickness (±10 %), total efficiency (±40 %), and beam dose (±20 %). Note that for an adequate description of cross-sections at low statistics the logarithm of values and error bars has to be used.

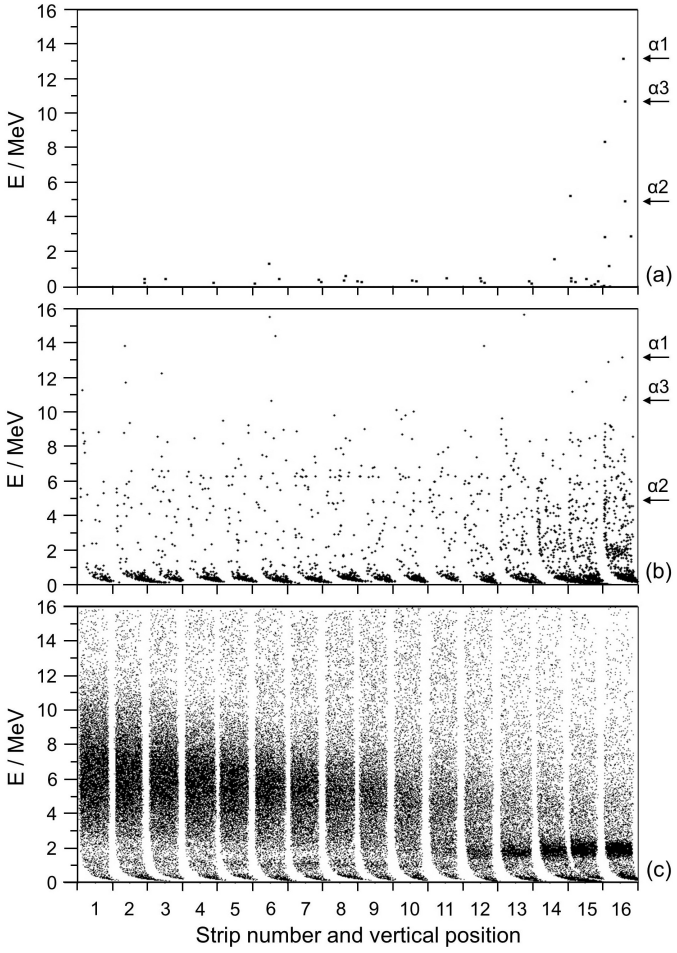

Fig. 8. Energy-position scatter plot of events measured with (a,b) and without (c) the anti-coincidence condition with both TOF and veto detector signals. The measuring time was 5 s in (a) and 10 min in (b,c) before and after the event α1 of the chain of the three signals from May 18, 2011. The spectra include events from both the 5.2-ms pulse and the 14.8-ms pause. The abscissa shows for each detector strip the vertical position ranging from 0 mm at the bottom to 35 mm at the top of the strip. For an explanation of the distribution of the background events see text. All three events of the chain are clearly seen on the upper half of detector strip 16 in (a), the first two also in (b) despite of the higher background. Note that α2 is an escape event for which only the energy loss in the stop detector is plotted. The event close to α3 in (b) has an energy of 10.857 MeV and a position of 26.0 mm. It occurred during the macro-pulse, 2.28 ms after its beginning and 393 s before α1. This event is in reasonable agreement with the background rate of such signals determined in sect. 3.2.3. and is, therefore, excluded as a member of the decay chain. Visible in (b) at 6.3 MeV and distributed across strip numbers 3 to 13 are also decays of the background activities of ^{240}Cm and ^{220}Rn.

3.2.1 The event α1 at 13.14 MeV

The event α1 of 13.14 MeV reveals the signature of a typical α decay. No coincidences with either the box or the Ge detectors were measured. The signal appeared in both the low energy and high energy analog electronics branch at 2,864 μs from the beginning of the macro-pulse. Signals having the same signature – occurrence during the macro-pulse and anti-coincidence to both TOF and veto detectors – appeared with a specific rate of 1.03×10^{-4} $s^{-1}mm^{-1}MeV^{-1}$ in strip 16 at the given vertical position and energy. This value gives the rate during the macro pulse, which is the relevant value needed for calculation of the probability that the event chain was created by chance. The average but wrong value would be lower by a factor of 5.2 ms/20 ms because the counting rate during the beam pauses is negligibly small. The event was measured with same energy as a single event also in the digital branch of the electronics.

The composition and distribution of the background is visualized in fig. 8. The lower part (fig. 8c) shows an energy-position scatter plot of all signals which occur during a time window of ±10 min around the 279-ms event chain. The data which occur in anti-coincidence to both the TOF and veto detectors within time windows of ±5 s and ±10 min are shown in figs. 8a and 8b, respectively.

The main intensity of events in fig. 8c is due to scattered beam particles decreasing from left (strip 1) to right (strip 16). These signals are strongly suppressed in the anti-coincidence spectrum. The peak at 2 MeV in strips 12 to 16 in fig. 8c is due to higher energy protons which traverse the stop detector, thus leaving only an energy loss signal. The distribution of signals up to about 10 MeV in strips 13 to 16 in fig. 8b is due to stopped protons and α particles. These protons and α's are produced in reactions with nuclei of Ti, O, and C being the components of the backing foil, the chemical compound of the target, and the charge equilibration foil downstream the target, respectively. They traverse through SHIP because of their high magnetic and electric rigidity and, therefore, occur primarily on the right side of the detector, which is closer to the beam axis.

For two reasons these particles are less suppressed in the anti-coincidence spectrum. Firstly, the efficiency of the TOF detectors is less for protons and α's compared to the heavier beam particles. Secondly, the veto detector has the same size as the stop detector. Therefore, protons and α's traversing the stop detector at the edge can be scattered out of the active area of the veto detector, see also fig. 3. The vertical alignment of the stop and veto detectors is not exactly the same which results in the lower suppression of the light particles at the lower end of detector strips 13 to 16.

The events along the line of constant energy of about 6 MeV in fig. 8b represent decays from the most intense α activities of implanted ^{240}Cm and ^{220}Rn nuclei which are in anti-coincidence with the TOF and veto detectors, see also fig. 7. The three signals which are subject of the discussion here, are marked. Note that α2 is an escape α with the residual energy measured in the box detector.

3.2.2 The composite event α2 at 11.81 MeV

The event α2 consists of a 4.94-MeV signal in strip 16 of the stop detector, which is in coincidence with a 6.88-MeV signal in segment 27 of the box detector (see fig. 3). The box detector was calibrated using an external α source of ^{239}Pu, ^{241}Am, and ^{244}Cm, thus recoil effects are avoided, but included is the energy loss in the inactive detector surface. These are the conditions under which escaped α's are measured in the box detector. The time difference between the two signals was located exactly at the center of the prompt coincidence peak having an FWHM of 125 ns. This coincidence event was measured during the beam-on period at 3,933 μs from the beginning of the macro-pulse, and it was again in anti-coincidence to both TOF and veto detectors. The event was also measured with same energies as a composite event in the digital branch of the electronics.

Unusual is the division of energy between the signals in the stop and box detector at the given geometry (see fig. 3). In the case that the α particle escapes from strip 16 and hits box segment 27 directly, it has to be emitted from a nucleus which is located at a depth of 52 μm in the stop detector. The value was determined as difference of the ranges of α particles with energies of 11.81 MeV (range 91 μm) and 6.88 MeV (range 39 μm) calculated with the computer code SRIM [65]. However, the implantation depth of ER's in our experiment is only at about 5 μm, see table 1.

Assuming as origin α emitters between lead and uranium, a kinetic energy of about 900 MeV is needed for an implantation depth of 50 μm. However, such high energies are not available at a beam energy of 325 MeV.

We also considered the possibility of pile-up of signals from fast α decays of nuclei above lead produced in inelastic reactions, *e.g.* the sequence ^{219}Ac–^{215}Fr. At a half-life of 90 ns of ^{215}Fr and escape of both α particles having energies of 8.66 and 9.36 MeV, respectively, the event α2 could be mimicked. We searched for events composed of a signal in strip 16 of the stop detector at a vertical position of (25.4±2.0) mm and a signal in any of the box-detector segments within a coincidence time of 5 μs with the condition that the sum of both energies is within a window from 10.8 to 12.8 MeV. The so determined specific rate, again during the beam-on phase, of true and chance events is 9.5×10^{-6} s^{-1}mm^{-1}MeV^{-1}. The reason for the small number is the low rate of true α decays and of background events which are not rejected by the anti-coincidence conditions at this detector position, see figs. 6 to 8.

In order to explain the division of energy of the composite event α2, we considered scattering of α particles in silicon. Using TRIM [65] we obtained the result that about 1 per thousand of 11.8-MeV α-particles is scattered so that the geometrical constraints are fulfilled. Because the calculated probability is small, we searched for similar measured events in the literature. Unfortunately, in more recent publications on SHN experiments, where bigger amounts of α decays from heavy nuclei were measured, the distribution of α energies between stop and box detector is not explicitly given. Also, the geometrical configuration is not given in general. Usually, escaped α events are marked as such and the sum energy is given with a larger error bar. Some examples, where the energy distribution is explicitly given, are listed in table 3. In most cases no signal was detected in the box detector indicating that the α particle escaped with high probability in backward direction through the opening of the box detector and thus almost perpendicular to the surface of the stop detector. The compilation reveals that from an estimated number of about 200 composite α events listed in the literature a fraction of a few percent, a factor of ten more than estimated using TRIM, has energies between 3 and 6 MeV in the stop detector, which is similar to the distribution of energies of the event α2.

3.2.3 The event α3 at 10.70 MeV

The event α3 was measured during the beam-on period at 2,311 μs after the beginning of a macro-pulse. Again, the signal was in anti-coincidence with both the TOF and veto detectors. The event was measured with energy and both positions in the low as well as the high amplification

Table 3. Literature values of escaped α particles having high energies in the stop detector. The total energy is from decays measured with full energy. The upper part of the table lists data from hot fusion reactions having less deep implantation depth. However, in all cases the implantation depth given by the reaction kinematics is typically 5 μm in hot and 10 μm in cold fusion reactions in which a 10-MeV α particle looses 0.45 or 0.90 MeV, respectively. The data in the table are ordered by the full energy of the α particles.

Isotope	E_{stop} /MeV	E_{box} /MeV	E /MeV	hot fusion/ cold fusion	Ref.
^{292}Lv	2.71	–	10.63	hot	[53]
^{281}Cn	2.32	7.86	10.18	hot	[66]
^{287}Fl	3.86	–	10.02	hot	[67]
^{284}113	2.01	8.03	10.00	hot	[68]
^{288}Fl	2.9	–	9.93	hot	[56]
^{272}Bh	3.14	5.83	9.02	hot	[68]
^{281}Ds	4.04	4.79	8.73	hot	[31]
^{272}Rg	4.61	–	10.99	cold	[69]
^{272}Rg	3.50	–	10.99	cold	[70]
^{262}Bh	6.4	–	10.37	cold	[45]
^{266}Hs	4.17	–	10.18	cold	[71]
^{257}Rf	2.11	–	9.02	cold	[72]
^{265}Sg	4.60	–	8.90	cold	[70]

branch of the analog electronics. It was also measured with same energy as a single event in the digital branch of the electronics.

Coincident with the α particle was a signal at an energy of 998 keV measured in Ge detector no. 4 within the 5 μs wide coincidence window. It was located in the time-to-amplitude converter (TAC) spectrum 265 ns (5.6 standard deviations) from the prompt peak having a width of $\sigma = \pm 47$ ns at α and γ energies of 10.7 and 1.0 MeV, respectively. The probability that true coincidences occur more than 5.6 standard deviations from the mean value is 6×10^{-7} % assuming a Gaussian distribution. Therefore, we consider the coincidence with the signal in the Ge detector as a chance event.

The specific rate of background events in the stop detector during the pulse and in anti-coincidence to TOF and veto detectors is 4.2×10^{-4} $s^{-1}mm^{-1}MeV^{-1}$ at the given energy and position of the event α3.

3.2.4 Search for an implanted ER prior to α1

True decay chains must begin with an implanted ER and, in the case of SHN, most likely by an SF event terminating the chain.

In the two dimensional energy-TOF spectrum, the ER's are expected to occur at energies higher than the target-like nuclei. Searching for an ER, we used an energy window from 20 to 45 MeV, thus considering energy loss in the dead layer of the detector and signal deficits by nuclear collisions during stopping. A time-of-flight value of 144 ns was estimated, which is given by the 780-mm distance between the TOF detectors and the ER velocity of 1.8 % of the velocity of light. The measured width of $\pm$7 ns corresponds to the velocity window of $\pm$5 % of SHIP. The rate of signals with these requirements and overlapping within a position window of (24.2 $\pm$ 3.0) mm with the position of the event chain is 0.10 s^{-1}, which corresponds to a mean interval of 10 s.

The three events closest to the chain fulfilling these conditions are marked ER1 to ER3 in table 2. They occur in intervals which are in agreement with the mean distribution of such signals. Therefore, the true ER cannot be determined unambiguously. However, the closest event ER1 occurring 5.4 s before α1 defines a lower limit of the lifetime, if losses of ER's between α1 and ER1 due to dead time of the electronics can be excluded.

In our case, each event, some are listed in table 2, creates a dead time of 16 μs. One of these events could be a reason for not detecting the true ER. At a counting rate of 770 Hz during beam pulses (200 Hz on average) the total dead time is 1.2 %, which represents the probability that the true ER is lost. The event closest to α1 occurred 2.264 ms before α1, which defines another limit of the lifetime of the implanted ER determined from our conventional analog signal processing.

Additional and less ambiguous information was obtained from the digital electronics. Signals from strip 16 were selected by analysis from signals of all other strips of the stop or segments of the box detector. Ten single events were measured between α1 and ER1. Due to the higher discriminator level of 1 MeV, this number is smaller than in the data measured with the analog electronics. The ten signals were also measured with position in the analog electronics, however, from the digital system pile-up events can be excluded, which could result in losses of data by dead time or distorted energy and position measurements within the analog system. Therefore, we can exclude the loss of an ER due to dead time effects during the period between α1 and ER1 because there were no pile-up events recorded.

Between signals α1 and α2, Δt = 261 ms, we measured 69 events. None of them occurred in detector strip 16. The three closest to α1 and α2 are listed in table 2. Between α2 and α3, Δt = 18 ms, four signals were measured. They are also listed in table 2. Again, none was measured in strip 16.

In conclusion, we state that the three signals α1, α2, and α3 follow each other directly at the same detector site. An ER correlated to the three-event chain cannot be determined unambiguously. The closest measured one (ER1) occurs 5.4 s before the event α1. However, this implanted nucleus is well in agreement with the distribution of accidental events having the properties of expected ER's. Therefore, it represents a lower limit of the lifetime of an implanted nucleus.

3.2.5 Search for α decays subsequent to α3 and an SF event terminating the chain

All previously measured decay chains of SHN produced in hot fusion reactions end by SF, which can, however, occur

minutes or even hours after the last α decay of the chain in some cases of odd and odd-odd nuclei [47,57,73,74].

The conditions for searching for possible SF events at the site of the event chain were 1) an energy signal in the range from 100 – 200 MeV, 2) a vertical position y = (y_0 ± 3.0) mm with y_0 = 24.2 mm in strip 16, and 3) an anti-coincidence with both the TOF and veto detectors. The mean rate of such events was 0.59 per day, and, thus, the mean interval 41 hours. The three subsequent events closest to the event chain fulfilling these conditions are listed in table 2 and marked by SF1 to SF3.

The event SF1 was measured 12 min after $\alpha 3$ and is completely within the focal plane stop detector. The ratio of a 12-min interval divided by 41 hours results in a probability of 0.0049 that SF1 occurred by chance. The distribution of the SF2 and SF3 events is compatible with a random one.

A signature for a true SF event is the coincidence with a signal in the Ge detectors resulting from fission-fragment γ rays. Such a coincidence was not observed in the case of SF1. In [75], we measured a probability of 0.12 that SF events of ^{252}No are registered without a signal from one of the crystals of the clover detector. Also measured in [75] was a probability of 0.60 that both SF fragments are stopped in the stop detector at an implantation depth of 4 to 5 μm. In such cases, no signal is obtained from the box detector as was the case for SF1.

The non-observation of coincident γ rays increases the probability to 0.041 (0.0049/0.12) that SF1 is a chance event. In this case, it could be explained by a projectile which lost energy due to scattering and which was not recorded by the TOF detectors.

If SF1 is interpreted as an SF event, then the measured energy of 159 MeV has to be corrected for energy losses in the inactive surface layer of the detector and energy deficits due to electron-hole recombination. From the study of SF events of ^{252}No [75] we estimate a total energy loss of 64 MeV which results in a total kinetic energy (TKE) of the event SF1 of (223 ± 35) MeV. This value agrees well with fission-fragment energies of SHN compiled in [66].

A search for a fourth α decay subsequent to $\alpha 3$ was performed within the interval of 721 s between $\alpha 3$ and SF1. The three events closest to $\alpha 3$ are listed in table 2. However, these events were in coincidence with the TOF detectors, had energies greater than 20 MeV and occurred in strips different from strip 16. The three events closest to $\alpha 3$ with signatures of radioactive decays measured in strip 16 within the position window of ±3 mm are also listed in table 2. All three signals occurred during the pulse, but they were in anti-coincidence to the TOF and the veto detectors. In addition, no coincident signal with the box and the Ge detector was measured.

Interesting is the first of these signals having an energy of 353 keV. It was measured 19.9 s after $\alpha 3$. Assuming an α particle escaping perpendicular to the surface of the stop detector at energies of 10.02 and 9.52 MeV corresponding to the decay of ^{287}Fl and ^{283}Cn, respectively, which are nuclei potentially populated by α decay of ^{291}Lv, we obtain ranges of 3.9 and 3.7 μm, traversed by the escaping α in the active layer of the detector. This range is in agreement with the ranges estimated for the implantation depth of ERs given in table 1, considering the uncertainties of implantation energies. The calculated energy losses in these Si layers are 351 and 333 keV [65], respectively, for 10.02 MeV α's and 366 and 347 keV for 9.52 MeV α's. These energy losses completely overlap with the measured energy of 353 keV.

The probability that an α particle escapes in backward direction without being registered in the box detector is about 15 %, see fig. 3. Another example for an event with similar properties is the previously overlooked decay of ^{283}Cn in the decay chain of ^{291}Lv. It will be discussed in sect. 4.4.

The mean time difference of signals with energies between 300 and 600 keV, which corresponds to energy losses of 10-MeV α particles emitted from nuclei implanted 3.3 to 6.5 μm, is 41 s. Therefore, the signal with energy of 353 keV measured 19.9 s after $\alpha 3$, cannot be definitely assigned to a member of the decay chain. It is also well in agreement with a chance event. Due to the higher energy, less probable for being α particles escaping in backward direction are the two signals at 1.98 and 3.99 MeV, see also sect. 3.2.2.

3.3 Calculation of the chance probability for the event chain $\alpha 1 - \alpha 2 - \alpha 3 -$ SF

The probability that the measured chain occurred accidentally was calculated according to eq. 5 in [64]. As time differences $\Delta t_{1,2}$ and $\Delta t_{2,3}$, we used the measured values for τ extracted from table 2. As rates λ_i, we used the specific rates given before in $s^{-1}mm^{-1}MeV^{-1}$. These rates were multiplied by a factor of 2 for $\alpha 1$ and $\alpha 2$, thus considering a reasonable energy window of ±1 MeV of the unknown α energy and by a factor of 0.42 in the case of $\alpha 3$, which corresponds to $\pm 3\sigma$ of the standard deviation of the measured α energy of ^{291}Lv [56], see table 4. The uncertainty of the position was taken into account by another factor of 2.6 determined from the range of ±1.3 mm in which the events occurred. All three rates are the rates during the macro-pulse, which are relevant here, because the three signals appeared during the beam-on periods.

As the measuring time, we took T = 763,776 s which is the total time of beam-on-target during the macro-pulse. During the pauses the background rates are considerably smaller and the increase of the chance probability can be neglected. The result is a probability of 4.4×10^{-8} that the chain of the events $\alpha 1 - \alpha 2 - \alpha 3$ was produced by chance. Doubling all energy and position windows still results in a small chance probability of 2.8×10^{-6}. Including the event SF1 reduces the probabilities by a factor of 0.041.

The small probability that the chain of three low energy events plus one high energy event was produced by chance favors the assignment to a true α-decay chain terminating by SF. However, the search for an implanted ER preceding $\alpha 1$ remains unsatisfactory. The nearest event with properties of an implanted ER was measured 5.4

Table 4. Summary of results of a review of even element isotopes. The rows are grouped according to α-decay chains (same N – Z value). The lower case letter n gives the number of observed events (see footnote (a)), b_α and b_{SF} are the measured values or limits of α or SF branching ratios. The capital letter T stands for the half-life, T^{exp}_{total} for the measured total half-life. The calculated partial α-decay half-life, T^{WKB}_α, was determined for transitions without change of angular momentum using the measured or extrapolated (see footnote (c)) Q_α values. Theoretical partial SF half-lives, T^{theo}_{SF}, are from [7,90] for even-even nuclei. In the case of even-odd nuclei the geometrical mean of the neighboring isotopes was used, in the case of odd-odd nuclei (last group listing N − Z = 64 nuclei) the geometrical mean of the four neighboring even-even nuclei. Odd particle hindrance factors are not included. The assignment of rows starting with the isotope in brackets is tentative. Data of the three event chain measured in this work and tentatively assigned to the decay of ^{299}120 are shown in bold. The notation 9.5e–2 stands for 9.5×10^{-2}. For references see text.

Isotope	n[a]	b^{exp}_α	b^{exp}_{SF}	E^{exp}_α /MeV	Q^{exp}_α /MeV	T^{exp}_{total}	T^{WKB}_α	T^{theo}_{SF}	T^{exp}_α/ T^{WKB}_α	T^{exp}_{SF}/ T^{theo}_{SF}
N − Z = 56, α-decay chain through ^{284}114										
^{284}114	3-3-0	≤0.25	1.0	10.61[b]	10.76	$2.0^{+2.7}_{-0.7}$ ms	8.8 ms	12 ms	≥0.91	0.17
N − Z = 57, α-decay chain through ^{285}114										
^{285}114	4-4-3	1.0	≤0.2	10.41±0.05	10.56	152^{+152}_{-51} ms	28 ms	132 ms	5.4	≥5.8
^{281}112	0-4-2	1.0	≤0.2	10.30±0.04	10.45	128^{+128}_{-43} ms	13 ms	49 ms	9.8	≥13
^{277}110	0-4-1	1.0	≤0.2	10.57±0.04	10.72	$4.1^{+4.1}_{-1.4}$ ms	0.72 ms	343 ms	5.7	≥0.06
^{273}108	0-4-4	1.0	≤0.2	9.53±0.04	9.67	765^{+765}_{-255} ms	93 ms	61 s	8.2	≥0.06
^{269}106	0-3-1	1.0	≤0.2	8.48±0.06	8.61	185^{+254}_{-68} s	33 s	14 min	5.6	≥1.1
^{265}104	0-3-0	≤0.2	1.0	–	7.8[c]	$61^{+\ 84}_{-\ 22}$ s	1.2 h	7.6 s	≥7.1e–2	8.0
N − Z = 58, α-decay chain through ^{286}114										
^{294}118	4-4-3	1.0	≤0.2	11.66±0.06	11.82	$0.69^{+0.69}_{-0.23}$ ms	0.36 ms	22 min	1.9	≥2.6e–6
(^{294}118)	1-1-0	≤0.5	1.0	–	–	$2.2^{+10.5}_{-\ 1.0}$ ms	–	22 min	–	1.6e–6
^{290}116	12-11-7	1.0	≤0.08	10.85±0.06	11.00	$8.3^{+3.6}_{-1.9}$ ms	8.0 ms	12 min	1.0	≥1.4e–4
(^{290}116)[d]	?-5-4	1.0	≤0.17	(10.85±0.08)	11.00	($0.32^{+0.26}_{-0.10}$ ms)	8.0 ms	12 min	0.040	≥2.6e–6
(^{290}116)[d]	?-6-3	1.0	≤0.14	(10.86±0.06)	11.01	($14.9^{+10.3}_{-\ 4.3}$ ms)	7.5 ms	12 min	2.0	≥1.5e–4
^{286}114	11-27-8	0.52	0.48	10.21±0.04	10.35	166^{+40}_{-27} ms	90 ms	1.5 s	3.55	0.23
^{282}112	1-14-0	≤0.07	1.0	–	10.1[c]	$0.96^{+0.35}_{-0.20}$ ms	104 ms	71 ms	≥0.13	0.014
N − Z = 59, α-decay chain through ^{287}114										
(^{299}/120)	**1-1-1**	**1.0**	**(≤0.5)**	**13.140±0.030**	**13.318**	–	**1.1 μs**	**39 ms**	–	–
(^{295}/118)	**1-1-1**	**1.0**	**(≤0.5)**	**11.814±0.040**	**11.976**	**$181^{+866}_{-\ 83}$ ms**	**0.16 ms**	**71 min**	**1130**	**≥8.5e–5**
^{291}116	3-3-2	1.0	≤0.25	10.74±0.07	10.89	$18^{+25}_{-\ 7}$ ms	14 ms	2.9 h	1.3	≥6.9e–6
(^{291}/116)	**1-1-1**	**1.0**	**(≤0.5)**	**10.698±0.030**	**10.847**	**$13^{+61}_{-\ 6}$ ms**	**18 ms**	**2.9 h**	**0.70**	**≥2.5e–6**
^{287}114	18-17-12	1.0	≤0.05	10.025±0.015	10.167	$0.54^{+0.17}_{-0.10}$ s	0.28 s	54 s	1.9	≥0.20
^{283}112	11-31-17	0.81	0.19	9.521±0.015	9.658	$4.48^{+0.98}_{-0.68}$ s	1.75 s	0.53 s	3.2	45
^{283}112	0-1-1	1.0	≤0.5	9.32±0.06	9.45	$3.8^{+18.1}_{-\ 1.7}$ s	7.0 s	0.53 s	0.54	≥14
^{283}112	0-1-1	1.0	≤0.5	8.94±0.07	9.07	$2.6^{+12.0}_{-\ 1.2}$ s	110 s	0.53 s	0.024	≥9.8
^{279}110	0-27-3	0.15	0.85	9.706±0.015	9.847	290^{+69}_{-47} ms	120 ms	26 ms	16	13
^{275}108	0-4-3	1.0	≤0.2	9.313±0.015	9.450	$201^{+201}_{-\ 67}$ ms	363 ms	0.51 s	0.55	≥2.0
^{271}106	0-4-1	0.25	0.75	8.53±0.08	8.66	96^{+96}_{-32} s	21 s	4.0 s	18	32
^{267}104	0-2-0	≤0.33	1.0	–	7.9[c]	$1.28^{+2.33}_{-0.50}$ h	0.46 h	5.8 s	≥8.3	794
N − Z = 59, α-decay chain through ^{287}114 (experiment VASSILISSA)[e]										
^{287}114	2-2-1	1.0	≤0.3	10.29±0.02	10.44	$5.5^{+9.9}_{-2.1}$ s	53 ms	54 s	104	≥0.34
^{283}112	4-6-0	≤0.14	1.0	–	9.9[c]	$308^{+212}_{-\ 89}$ s	360 ms	0.53 s	≥6100	581

Table 5. Table 4 continued.

Isotope	n[(a)]	b_α	b_{SF}	E_α^{exp} /MeV	Q_α^{exp} /MeV	T_{total}^{exp}	T_α^{WKB}	T_{SF}^{theo}	$T_\alpha^{exp}/T_\alpha^{WKB}$	$T_{SF}^{exp}/T_{SF}^{theo}$
N − Z = 60, α-decay chain through ^{288}114										
^{292}116	10-8-4	1.0	≤0.09	10.628±0.015	10.776	$12.8^{+7.0}_{-3.3}$ ms	27 ms	40 h	0.47	≥9.9e–7
^{288}114	24-32-20	1.0	≤0.03	9.934±0.015	10.074	644^{+138}_{-97} ms	478 ms	35 min	1.3	≥1.0e–2
^{284}112	0-32-0	≤0.03	1.0	–	9.6[(c)]	118^{+24}_{-17} ms	2.6 s	4.0 s	≥1.5	0.029
N − Z = 61, α-decay chain through ^{289}114										
^{293}116	6-5-5	1.0	≤0.14	10.559±0.015	10.705	57^{+46}_{-18} ms	39 ms	39 d	1.5	≥4.2e–9
^{289}114	9-15-12	1.0	≤0.06	9.836±0.015	9.974	$1.87^{+0.65}_{-0.38}$ s	0.87 s	7.7 h	2.1	≥1.1e–3
(^{289}114)	0-1-1	1.0	≤0.5	9.848±0.030	9.987	640^{+3000}_{-290} ms	0.87 s	7.7 h	0.03	≥9.7e–6
^{289}114	0-1-1	1.0	≤0.5	9.48 ±0.08	9.61	$1.4^{+6.6}_{-0.6}$ s	9.6 s	7.7 h	0.15	≥1.0e–3
^{285}112	0-15-12	1.0	(0.06)	9.189±0.015	9.320	$28.9^{+10.1}_{-5.9}$ s	16 s	86 s	1.8	(5.1)[(f)]
^{285}112	0-1-1	1.0	≤0.5	9.03 ±0.08	9.16	$1.6^{+7.7}_{-0.7}$ s	52 s	86 s	0.03	≥3.7e–2
^{281}110	0-15-1	0.07	0.93	8.727±0.030	8.853	$13.0^{+4.5}_{-2.7}$ s	105 s	0.14 s	1.8	100
^{277}108	0-1-0	≤0.5	1.0	–	9.0[(c)]	$3.1^{+14.9}_{-1.4}$ ms	7.5 s	6.7 ms	≥8.3e–4	0.5
N − Z = 62, α-decay chain through ^{290}114 (tentative[(g)])										
(^{290}114)	1-1-1	1.0	≤0.5	9.710±0.045	9.846	21^{+101}_{-10} s	1.9 s	4.3 d	11	≥1.1e–4
(^{286}112)	0-1-1	1.0	≤0.5	8.670±0.045	8.793	640^{+3100}_{-300} s	782 s	1950 s	0.82	≥0.67
(^{282}110)	0-1-1	1.0	≤0.5	8.83 ±0.18	8.96	67^{+320}_{-30} s	47 s	1.5 s	1.4	≥89
(^{278}108)	0-1-0	≤0.5	1.0	–	8.8[(c)]	690^{+3300}_{-310} s	32 s	0.98 ms	≥43	7.0e+5
N − Z = 64, α-decay chain after EC of ^{290}114 (tentative[(g)])										
(^{290}114)	EC	≤0.5	≤0.5	–	9.9[(c)]	19^{+91}_{-9} s[(h)]	1.4 s	4.3 d	≥27	≥1.0e–4
(^{290}113)	1-1-1	1.0	≤0.5	9.710±0.045	9.846	$2^{+9.6}_{-0.9}$ s[(h)]	0.87 s	64 d	2.0[(h)]	≥7.2e–7
(^{286}111)	0-1-1	1.0	≤0.5	8.670±0.045	8.793	640^{+3100}_{-300} s	326 s	2.2 h	2.0	≥0.16
(^{282}109)	0-1-1	1.0	≤0.5	8.83 ±0.18	8.96	67^{+320}_{-30} s	20 s	3.3 s	3.4	≥41
(^{278}107)	0-1-0	≤0.5	1.0	–	7.9[(c)]	690^{+3300}_{-310} s	4.7 h	2.4 ms	≥0.081	2.9e+5

[(a)] Number of parent nuclei of observed decay chains - number of events used for mean value of half-life - number of events used for mean value of α energy. Energies from escaped α particles having large error bars were not used for determining the mean values.
[(b)] Alpha energy of ^{284}Fl estimated by extrapolation of the measured α energies of ^{285}Fl and ^{286}Fl, see fig. 9.
[(c)] Q-alpha values estimated by extrapolation of data shown in fig. 26 in [91].
[(d)] Decays of ^{290}116 tentatively divided into two groups with different half-lives.
[(e)] Data measured at VASSILISSA, which were assigned to ^{287}Fl and ^{283}Cn [86,87,89].
[(f)] HF_{SF} value obtained from tentatively assigning an 9.848-MeV α − SF chain measured in [77] to ^{289}Fl − ^{285}Cn.
[(g)] Arguments as discussed in sect. 5.1.2 favor an assignment to an α-decay chain starting at ^{290}113 which is populated by EC decay of ^{290}Fl.
[(h)] The measured lifetime of 21 s between implantation of CN and first α decay was divided between EC and α decay assuming $HF_\alpha = 2$, see text in sect. 5.1.2.

s before $\alpha 1$, which is too long for an unhindered α decay of 13.14 MeV. In addition, the rate of chance events with similar properties is 0.10 s^{-1}. Therefore, the event ER1 cannot be distinguished from a chance event. Due to these uncertainties, we reviewed all measured data of even-element SHN, which were published in recent years, aiming to provide systematics of experimental results, which could be useful for an assignment or at least for a better understanding of the measured data. This review was performed despite the low probability that the event chain $\alpha 1 - \alpha 2 - \alpha 3$ was produced by chance.

4 Review of known data

We performed a critical review of all data of even elements measured in relevant hot fusion reactions since 1998. It was necessary to make this review, because new data became available since the 2007 review [57] and previously measured but later not confirmed data or tentatively assigned data are in general no longer considered in later evaluations. Data published in [31,53,56,66,67,75–89] were reviewed. We organize the discussion in subsections entitled by nuclei of the same N – Z value. These are the nuclei which are populated within an α-decay chain. A summary with those of the three-event chain embedded is given in table 4. A graphic presentation of the α energies is shown in fig. 9.

The mean values of the α energies are given in column 5 of table 4. They were determined as a weighted mean from the more precise values of α's slowed down in the stop detector. Given error bars are those of the most accurate measurements thus avoiding too small error bars emerging from the averaging, which could become smaller than the systematic uncertainties. For fissioning nuclei at the end of the α-decay chains, Q-alpha values were estimated by extrapolation of data shown in fig. 26 in [91].

Measured total half-lives are given in column 7. From these the partial α or SF half-lives can be determined using the corresponding measured branching ratios given in columns 2 and 3. Limits of SF branchings are determined under the assumption that the n+1 decay of the n measured α decays is an SF event and, *vice versa,* for limits of α-decay branchings.

Alpha half-lives were also calculated from the measured α energies using the tunneling probability through the Coulomb barrier as described in [53], p. 18 and briefly in sect. 4.4 in this work. The values are listed in column 8 marked as T_α^{WKB}. All values were calculated with a centrifugal barrier of zero. Most of the theoretical values agree reasonably well with the measured values. The ratio between experimental and calculated partial half-lives gives the α-decay hindrance factor HF_α listed in column 10. Analogous, SF hindrance factors HF_{SF} given in column 11 were calculated as ratio between measured and calculated partial fission half-lives with the calculated values taken from [7,90] and listed in column 9.

4.1 Decay chain N – Z = 56 through ^{284}Fl

Alpha decay of N – Z = 56 SHN would terminate by SF of the known nucleus ^{260}No. However, the only known isotope of the nuclei beyond No is ^{284}Fl which was identified only recently in reactions with targets of ^{239}Pu and ^{240}Pu [66]. The isotope decays by SF with a half-life of 2.0 ms. The systematics of Fl α energies allows for an extrapolation of measured energies, see fig. 9, resulting in an energy of 10.61 MeV for ^{284}Fl. Using this energy, a partial α-decay half-life of 8.8 ms is calculated from which an α branching of 23 % follows, see table 4. This value is large enough for possibly observing this decay mode and therefore the population of the daughter ^{280}Cn, which most likely fissions, in future experiments.

4.2 Decay chain N – Z = 57 through ^{285}Fl

Only a single α-decay chain was measured in the reaction ^{242}Pu(^{48}Ca,5n)^{285}Fl in [76]. However, the first α decay of the chain escaped, and only the lifetime was determined. The data were confirmed using the reaction ^{240}Pu(^{48}Ca,3n)^{285}Fl in 2014 [66]. Three decay chains were measured, now providing also the α energy of ^{285}Fl. Mean values of the data are given in table 4 and plotted in fig. 9 at N – Z = 57.

4.3 Decay chain N – Z = 58 through ^{286}Fl

The N − Z = 58 and also the N − Z = 60 decay chains connect even-even nuclei where in general the α transitions occur between ground-states. For each nucleus only one transition with well defined α energy was measured, see fig. 9. In both cases the chains end by SF of copernicium isotopes at the latest. For the N − Z = 58 nuclei SF was also measured for ^{286}Fl but not for the − Z = 60 nucleus ^{288}Fl.

A total of 29 N − Z = 58 decay chains are published. Fourteen end by SF of ^{282}Cn, in one case fission was missed after α decay of ^{286}Fl. Thirteen chains end by SF of ^{286}Fl, in no case the chains extended below ^{282}Cn. In one case ^{282}Cn was produced directly in a reaction with ^{238}U. An SF branching of 100 % and a half-life of $(0.96^{+0.35}_{-0.20})$ ms of ^{282}Cn is deduced.

Twenty seven decays were assigned to ^{286}Fl, 14 α decays and 13 SF events, resulting in branchings of 52 and 48 %, respectively. No difference of lifetimes is observed, whether ^{286}Fl is produced directly (11 chains) or by α decay of ^{290}Lv (16 chains). From the 27 events a mean half-life of (166^{+40}_{-27}) ms follows. In five cases α decay of the preceding ^{290}Lv was missed. In these cases a lifetime of 12 ms was subtracted from the measured time difference between implantation of ^{290}Lv and α decay of ^{286}Fl thus taking into account the lifetime of ^{290}Lv.

The isotope ^{290}Lv was populated 12 times in the reaction ^{245}Cm(^{48}Ca,3n)^{290}Lv. However, the α decay was observed only 7 times. Four times the isotope was populated by α decay of ^{294}118. The distribution of lifetimes

of the 11 decays of ^{290}Lv is rather broad. According to a statistical analysis descibed in [92], the standard deviation σ of Θ_{exp} for one common lifetime is 2.13 instead of 1.17 and thus the probability for such an assignment is smaller than 5 %. Agreement with the statistical distribution is obtained by dividing the events into two groups with lifetimes smaller than 5 ms (5 decays) and larger than 5 ms (6 decays). The resulting half-lives are given in brackets in table 4. However, because the α energies of the two groups agree within error bars, the information for separation of the events into two groups is not sufficient.

It is interesting to note that among the decays of ^{290}Lv a lifetime of 0.098 ms was measured which was much shorter than the average of $(12.0^{+5.2}_{-2.7})$ ms. However, the α energy agrees with the mean value. A similar extremely short lifetime of 0.076 ms was measured in the case of ^{292}Lv, which has a mean lifetime of $(18.5^{+10.1}_{-4.8})$ ms. In both cases, these results may reflect the broad scattering of events following an exponential distribution.

Four decay chains were measured in the ^{249}Cf(^{48}Ca,3n) ^{294}118 reaction, three of these ended by SF of ^{286}Fl and one by SF of ^{282}Cn. The half-life and α-decay energy of ^{294}118 are given in table 4.

The mean values of α energies of ^{294}118, ^{290}Lv, and ^{286}Fl were determined from 3, 7, and 8 events, respectively, see table 4 and fig. 9.

One SF event with a lifetime of 3.16 ms originally assigned to ^{294}118 was observed in the reaction ^{48}Ca + ^{249}Cf [82]. This event is not confirmed.

4.4 Decay chain N – Z = 59 through ^{287}Fl

Nuclei of this chain were produced in reactions with ^{238}U (^{283}Cn, 3n channel, 11 chains), ^{242}Pu (^{287}Fl, 3n, 17 chains), ^{244}Pu (^{287}Fl, 5n, 1 chain), and ^{245}Cm (^{291}Lv, 2n, 3 chains). Odd-N nuclei are populated and the measured α energies reveal a more pronounced structure compared to the even-N isotopes.

Three long lifetimes of 4836, 3255, and 13909 ms, which are considerably longer than the mean value, were assigned to SF of ^{279}Ds [83]. In that work it was assumed that the preceding α decay of ^{283}Cn was missed. However, with the more comprehensive set of data now available, it seems reasonable that indeed the SF of ^{283}Cn was observed. Likely, the circumstances are similar in a fourth case where SF was observed with a lifetime of 776 ms, but with no preceding α decay. A re-assignment of SF in these four cases to ^{283}Cn is corroborated by the observation of two SF decays from a total of four events observed in [75], whereas no fission event from a total of 27 decay chains was assigned to ^{283}Cn in [56,83,85]. With the new assignment we obtain reasonable lifetimes for both ^{283}Cn and ^{279}Ds and a reasonable SF branching of 19 % of ^{283}Cn, see table 4.

A half-life of $(4.48^{+0.98}_{-0.68})$ s for ^{283}Cn was determined from 31 decays. Six of them decay by SF resulting in an SF branching of 19 %. A half-life of $(0.54^{+0.17}_{-0.10})$ s for ^{287}Fl was determined from 17 decays. Spontaneous fission of this nucleus was not observed and in three cases out of twenty, the α decay was missed. It is interesting to note that two short lifetimes of 0.012 s and 0.009 s were also observed, however, the α energies of these events agree with the mean value of all other decays of ^{287}Fl indicating statistical fluctuations. A half-life of (18^{+25}_{-7}) ms for ^{291}Lv was determined from 3 decays. Spontaneous fission of this nucleus was not observed. Mean values of the α energies of ^{291}Lv, ^{287}Fl, and ^{283}Cn were determined from 2, 12, and 17 decays, respectively, which all, for each nucleus, agree within error bars. The values are given in table 4 and plotted in fig. 9.

In three cases out of the 26 α decays of ^{279}Ds published, relatively long decay chains terminated by SF at ^{267}Rf (two chains) and ^{271}Sg (one chain). Data of these chains were included in determining mean values (larger symbols at N – Z = 59 in fig. 9 marking six consecutive α decays from ^{291}Lv to ^{271}Sg). A more detailed discussion is given below.

Note that there exists an α-decay energy inversion at elements 112 and 110, also observed for the N – Z = 57 decay chain. The reason is the stronger binding of Z = 108 isotopes due to a large level gap at this proton number at deformation, resulting in the high Q_α value of Z = 110 isotopes. However, the strength of this level gap seems to vanish at N – Z = 61 where in one decay chain continuously decreasing α energies were measured from ^{293}Lv to ^{281}Ds.

One α-decay chain starting with a first α energy of 10.502 MeV was measured in our previous irradiation of ^{248}Cm with ^{48}Ca [53]. The α energy was in good agreement with known α energies of ^{293}Lv [83,84], whereas the decays of the daughter nuclei were different. A tentative assignment was made to ^{293}Lv (N – Z = 61) and population of isomeric levels in the daughter nuclei were suggested.

Comparing the α energies of the three long chains at N – Z = 59 with those of the long decay chain assigned tentatively to ^{293}Lv in our previous work [53], we observed good agreement with α decays of ^{287}Fl, ^{279}Ds, and ^{275}Hs. The energies are plotted most right of the N – Z = 59 group in fig. 9. In this case, however, the α decay of ^{283}Cn is missing. A reinspection of the data measured in 2010 revealed an escape α at an energy of 244 keV between the signals of 10.029 and 9.707 MeV, 1718 ms after the 10.029-MeV signal, see table 5 in [53]. The interval to the subsequent 9.707 MeV α particle is 4048 ms.

Due to the low energy, no position signal was measured. However, the signal occurred during the low background period of the macro pause at 13.495 ms. It was the only signal from a total of 35 in strip number 4 (see [53]) occurring during the 5766-ms interval between the two α's of 10.029 and 9.707 MeV during the pause. All other 34 signals occurring during beam pulses were in coincidence with signals from the TOF detectors. Therefore, an assignment of the low energy signal to an α decay of the granddaughter ^{283}Cn of ^{291}Lv is reasonable. The assignment is corroborated by the following arguments.

The full energy of the escaped α particle was estimated using a relation between energy of α particles and half-life.

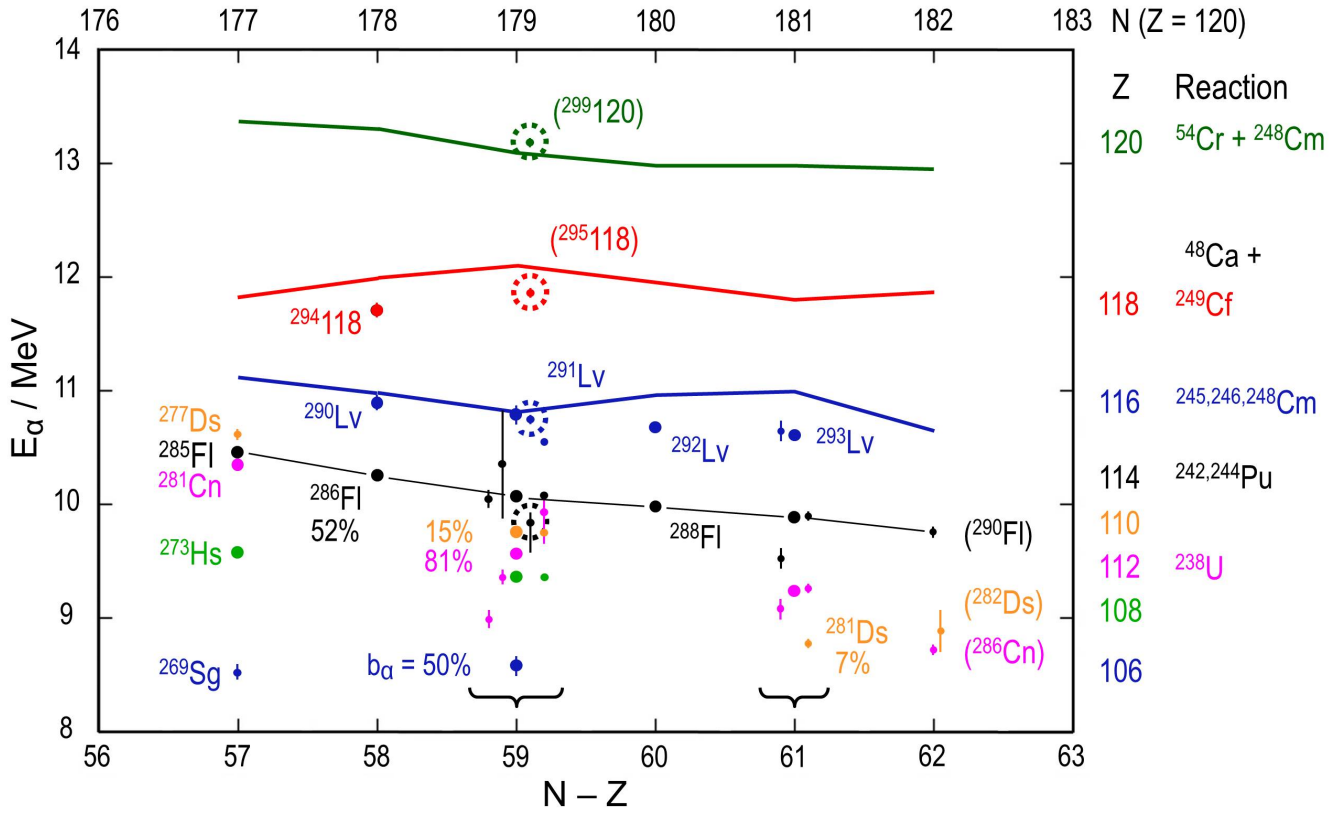

Fig. 9. Systematics of experimental α energies. The data are taken from table 4. They are grouped for nuclei within an α-decay chain (same N – Z value). Large dots represent data from mean values (see table 4), small dots from single α-decay chains. In most cases the error bars are smaller than the symbols. The α energies of ^{287}Fl and ^{283}Cn with asymmetric error bars were calculated from the measured lifetimes. Also given are the α-branching ratios in percent if the values are smaller than 100 %. Tentative assignments are given in brackets. Not shown are the terminating nuclei which decay by SF. Alpha energies of the N − Z = 59 chain tentatively assigned to the decay of ^{299}120 are encircled with dotted lines. Alpha energies of a chain tentatively assigned to ^{290}Fl are shown at N − Z = 62. An alternative explanation based on EC of ^{290}Fl is also given. In this case the chain of odd-odd nuclei starting with ^{290}113 would belong to the group of N − Z = 64 nuclei. Thick lines connect theoretical α energies for isotopes of the elements 116, 118, and 120 [55,93,94], the thin line connecting isotopes of Fl is drawn to guide the eye.

For calculation of the partial α half-lives we calculated the reduced α widths for the given nuclei, in this case ^{283}Cn, and normalized these to the width of the 0.3 μs decay of ^{212}Po. The barrier penetrability was calculated using the WKB method (Wentzel-Kramers-Brillouin, see [95]) with the α-nuclear potential given in [96]. In addition, a hindrance factor $HF_\alpha = 3.2$ was assumed, which was obtained from 31 known α decays of ^{283}Cn, see table 4. The method is justified by the good agreement between measured and calculated lifetimes given for known transitions in table 4.

The value of $(9.76^{+0.09}_{-0.27})$ MeV obtained is consistent within experimental uncertainties with the measured value of 9.52 MeV of ^{283}Cn given in table 4, see also fig. 9. The asymmetric error bars were determined from the upper and lower limit of the lifetime of $\tau = (1.72^{+8.23}_{-0.78})$ s valid for one-event statistics presented in [64].

Assuming emission of a 9.52-MeV α particle, we calculated the path of the escaped α particle in the active detector layer from the measured energy loss using ranges determined with the computer code SRIM [65]. The result is 2.6 μm in silicon. The obtained value of 2.6 μm is in agreement with an estimate of the implantation depth of the ER of about 2.3 μm taking into account the 3.5 μm Mylar degrader foil in front of the detector used at the time of the event. The agreement between the two values reveals that the α particle emitted from ^{283}Cn escaped almost perpendicular from the detector surface.

The event chain was measured during irradiation of ^{248}Cm with ^{48}Ca at a beam energy resulting in E* of 40.9 MeV of the CN ^{296}Lv. For the production of ^{291}Lv, the evaporation of 5 neutrons would be necessary, which is rather unlikely at this E*. A 5n channel was observed at 52.5 MeV in the reaction ^{48}Ca + ^{244}Pu in [56] (see also fig. 4 in [53], which shows measured and calculated excitation functions of the reaction ^{48}Ca + ^{248}Cm). However, considering the target impurity, we also have to take into account a reaction with the 3.10 % contamination of ^{246}Cm. In this case, the CN ^{294}Lv has E* of 39.4 MeV and

the isotope ^{291}Lv is produced in a 3n channel. The measured cross-section is (27^{+63}_{-23}) pb. This value seems very large for a hot fusion reaction. However, considering the large statistical uncertainty resulting in a lower 68 % limit of 4 pb, which almost overlaps with the value of $(0.9^{+2.1}_{-0.7})$ pb measured for the 3n channel at the same beam energy in the reaction with ^{248}Cm, then the assignment of this decay chain to ^{291}Lv seems reasonable. The α energies of the chain are marked rightmost from the mean values at N – Z = 59 in fig. 9.

With this assignment, the α energy of ^{291}Lv of this single chain is (238±70) keV lower than the mean values of the other three ^{291}Lv α energies, see table 4. Similarly, lower α energies were measured in two cases for the isotope ^{283}Cn. These lower energies of (8.94±0.07) and (9.32±0.06) MeV were measured after decay of ^{287}Fl [83]. They are considerably lower than the mean value of (9.521±0.015) MeV. The data are plotted to the left of the larger symbols of the mean values at N – Z = 59 in fig. 9. Their decay constant, however, agrees with the mean value.

In the cases where α energies lower than the mean value were measured, it seems reasonable that the α transition populates excited levels in the daughter nucleus. An impression of possible transitions in nuclei located in the region of interest here is given in fig. 11 of [53], where the calculated level schemes of N – Z = 61 nuclei (^{293}Lv) are plotted.

In six cases, long living nuclei with lifetimes between 52 and 1459 s having a mean value of 446 s were assigned to SF of ^{283}Cn [86,87,89]. These data differ considerably from all other measurements and will be discussed in sect. 5.2.

4.5 Decay chain N – Z = 60 through ^{288}Fl

All N – Z = 60 decay chains end at ^{284}Cn by SF. A total of 34 SF decays are known and the resulting half-life determined from 32 events is (118^{+24}_{-17}) ms. In two cases the parent α decay was missing.

The isotope ^{288}Fl was produced 23 times in reactions with ^{244}Pu, one time with ^{242}Pu and ten times as daughter of ^{292}Lv produced in reactions with ^{248}Cm. A half-life of $(644^{+138}_{-\ 97})$ ms was determined from 32 α decays.

The half-life of $(12.8^{+7.0}_{-3.3})$ ms of ^{292}Lv was determined from eight events. In one case out of the ten produced chains the ER and in one case the α decay was missed. One α decay has a short lifetime of 0.076 ms. However, it was considered in the half-life determination, because all other properties of the chain are in agreement with the mean values.

The weighted mean values of the α energies of ^{292}Lv and ^{288}Fl neglecting escape events, are given in table 4. Only one α energy of (9.848 ± 0.030) MeV for ^{288}Fl [77] (not shown in fig. 9) is 86 keV lower than the mean value of (9.934 ± 0.015) MeV determined from twenty decays. Low energy levels in the daughter ^{284}Cn, which could be populated by α decay, are not expected in transitions between even-even nuclei at a calculated deformation β_2 value of 0.089 [97]. On the other hand, the α energy would be in good agreement with the decay of ^{289}Fl having a mean α-decay energy of (9.836±0.015) MeV. The parameters of the 9.848-MeV event are tentatively listed in the group of N − Z = 61 chains with the isotope ^{289}114 in brackets. This isotope could emerge from a 3n channel in the reaction ^{48}Ca + ^{244}Pu used in [77]. In this case, the subsequent daughter decay would be the first observation of a SF branching of ^{285}Cn. The resulting HF_{SF} value would be 5.1, which is well in the range of measured HF_{SF} values for N − Z = 57 and 59 and other N − Z = 61 nuclei (see table 4 and sect. 5.1.2).

4.6 Decay chain N – Z = 61 through ^{289}Fl

Eight decay chains of ^{289}Fl were observed in reactions with ^{244}Pu, all of them are terminating by SF at ^{281}Ds. A ninth chain, shown by small dots to the right of the mean values in fig. 9, proceeds to ^{277}Hs where it terminates by SF.

Six decay chains of ^{293}Lv were observed in reactions with ^{248}Cm, again all of them are terminating by SF at ^{281}Ds. One of these chains exhibits a significantly lower α energy of 9.48 MeV of ^{289}Fl. Also the α energy of ^{285}Cn is slightly below the mean value, see small dots to the left of the mean value in fig. 9. Half-lives and α energies of the members of all other chains agree. The mean values are given in table 4 and are plotted in fig. 9.

A previous tentative assignment of a chain to ^{293}Lv observed in the reaction ^{48}Ca + ^{248}Cm [53] was discussed before in sect. 4.4.

4.7 Decay chain N – Z = 62 through ^{290}Fl

One chain originally assigned to ^{289}Fl produced in a 3n channel in the reaction ^{48}Ca + ^{244}Pu [31] does not fit from the energy point of view to any of the decay chains with N – Z ≤ 61. However, it fits well into the systematics, if assigned to ^{290}Fl, see fig. 9. In this case the isotope would have been produced in a 2n channel. Based on the presently known extensive data on excitation functions, see fig. 8 in [73], a 2n channel seems reasonable, because a relatively low beam energy was chosen in [31], which resulted in E* of only 35 MeV.

However, in this case it is difficult to understand the measured long SF half-life of $(11.5^{+55.0}_{-\ 5.2})$ min of ^{278}Hs terminating the chain. The neighboring even-odd isotope ^{277}Hs has a measured SF half-life of only 3.1 ms. The calculated SF half-life for ^{278}Hs is 0.98 ms. A possible explanation for the occurrence of the measured long SF half-life is given in sect. 5.1.2 assuming EC of ^{290}Fl. This possibility is indicated as an alternative decay channel in fig. 9. In this case the chain of odd-odd nuclei starting with ^{290}113 would belong to the group of N − Z = 64 nuclei.

The re-assignment to the 2n channel could be confirmed by synthesis of ^{294}Lv in the reaction ^{248}Cm(^{48}Ca,2n)^{294}Lv using a low beam energy. The N − Z = 62 decay chain is the most neutron rich one, which can be directly produced with stable beams apart from an irradiation of

the extremely difficult to produce target of ^{257}Fm, see fig. 1. In that reaction the 2n channel would have an N − Z value of 63. In sect. 5.1.2 we will see that in certain cases EC offers another possibility for population of more neutron rich nuclei.

5 Discussion

In irradiation of a ^{248}Cm target with ^{54}Cr ions, three signals were measured which are correlated in position and time within 279 ms. A statistical analysis revealed that the sequence of signals did not occur by chance with high probability. The anti-coincidence conditions to both TOF detectors and the veto detector identify the signals with high probability as decay products. The assignment of an implanted nucleus starting and of an SF event terminating the chain cannot be determined unambiguously. However, as we have seen in the previous section, incomplete or not yet fully understood decay chains were also observed several times in other SHN experiments.

In this section, we will discuss the results of previous experiments and the properties of the new chain in the framework of physical expectations. Assuming synthesis of isotopes of element 120 in the reaction ^{54}Cr + ^{248}Cm, at the given projectile energy of 305 MeV (E* = 41.9 MeV, see table 1) the evaporation channels 2n, 3n, and 4n are open. In the case of 4n, the known nuclei ^{294}118 and ^{290}Lv are populated, which have different α-decay energies than those observed, see table 4 and fig. 9. So far, 2n channels were observed in the reaction ^{48}Ca + ^{243}Am at E* of 33.8 and 34.2 MeV [98] and possibly in the reaction ^{48}Ca + ^{244}Pu at 35 MeV [31], see sect. 4.7. These E* values are more than 7 MeV lower than the value of the reaction studied here, which makes a 2n channel very unlikely. In addition, the α energy of ^{292}Lv is 2σ lower than the energy of the third signal measured here, see table 4 and fig. 9. Good agreement with both E* and within error bars of the α energy of ^{291}Lv were obtained in the case of the 3n channel, which means population of the isotope ^{291}Lv by sequential α decays of ^{299}120 and ^{295}118.

Most striking during the analysis of the raw data was the good agreement of the measured Q_α values with the predictions for the α decay of ^{299}120 and ^{295}118. In fig. 10a we show for N – Z = 59 nuclei (α-decay chain through ^{291}Lv) a comparison of experimental and theoretical Q_α values. Experimental data from ^{271}Sg to ^{291}Lv are the results of data originally measured at FLNR, see sect. 4.4. The theoretical values are from calculations using the MM models of Sobiczewski *et al.* [54,55] (MM-S) and Möller *et al.* [9] (MM-M), the chiral mean-field model of Schramm [37] (CMF), and the semi-empirical shell model of Liran *et al.* [99] (SE). The perfect agreement with the predictions of the MM models is surprising.

The trend of increasing Q_α values up to ^{303}122 is also obtained in the framework of the CMF model, whereas the SE model having an assumed shell closure at Z = 126 results in decreasing Q_α values when Z = 126 is approached. However, the values of ^{291}Lv and the lighter nuclei are well reproduced also in this model.

Experimental and theoretical data of the neighboring decay chains starting at ^{294}118, ^{292}Lv, ^{293}Lv, and ^{294}Lv were discussed in detail in sect. 4.3 in [53]. Also for these chains similar trends as shown in fig. 10a were established.

5.1 Decay properties of known nuclei

5.1.1 Alpha-decay half-lives

Whereas the energies of the three events are well in agreement with the theoretical predictions, the lifetimes need to be discussed critically. In table 4, we listed all measured α-decay half-lives of even element isotopes and compare them with calculated values using as input the measured α energy. The calculation is based on the WKB method, described in [53]. An advantage of the method is that a centrifugal barrier can be added to the Coulomb potential and, thus, changes of angular momenta between mother and daughter nuclei can be included quite naturally.

The WKB half-lives in table 4 are calculated with angular momentum zero. Alpha-decay hindrance factors HF_α are determined as ratio between measured and calculated half-lives. As expected, no or only small hindrance is observed in the case of even-even nuclei within error bars. The relatively high hindrance factor of 3.55 of ^{286}Fl indicates possibly a value of the measured α-decay branching that is too small.

No reason is found for the short half-life of the subgroup of five events of ^{290}Lv resulting in $HF_\alpha = 0.04$. As long as no additional information is available, the seeming enhancement has to be assigned to statistical fluctuation.

The assignment of one event with lower energy to ^{288}Fl (not listed in table 4) observed in [77] is doubtful, because a low energy level at 86 keV is not expected in the even-even daughter ^{284}Cn. However, the energy would agree well with the decay of ^{289}Fl.

Odd-A nuclei of N – Z = 59 and 61 have HF_α values between 1 and 3 in all cases when the half-lives were determined from more than two events, except the two nuclei ^{279}Ds and ^{271}Sg which have HF_α values of 16 and 18, respectively. In these two cases, the number of measured α decays is low and thus the statistical uncertainty high. It seems possible that values of measured b_α that are too small are responsible for the increase of the partial α half-life resulting in the high HF_α values.

Interestingly, the nuclei from ^{285}Fl to ^{269}Sg of the N – Z = 57 chain all have similar HF_α values which are a factor of about three higher than those of the odd-A chains discussed before. A change of angular momentum $\Delta l = (4 \pm 1)\,\hbar$ could explain the longer experimental half-lives of these five nuclei of the decay chain from ^{285}Fl to ^{269}Sg. Note that this chain is the most neutron deficient one of the nuclei discussed here. It is located in a region of transitional nuclei between spherical SHN and deformed nuclei around Z = 108, N = 162 where the order of high and low spin quasi-particle neutron levels could reduce the probability of α decay.

For the α decay at 10.29 MeV of the VASSILISSA experiment [89], which was assigned to ^{287}Fl, an HF_α value

of 104 is determined. Such a strong hindrance could be explained by a change of angular momentum $\Delta l = (8 \pm 2)\,\hbar$. In this case, the result could be due to the existence of an isomeric level which can decay only when the α particle is emitted with a large amount of angular momentum.

Of special interest for future studies using further improved experimental techniques are the few events having α energies and/or half-lives different from the majority of measured decays of nuclei to which they were assigned. In table 4, they stand out due to their HF_α values below 1, which, in this case means a seeming enhancement of the decay probability. The reason could be that a low intensity transition represents a small decay branch of the level decaying with higher intensity at another energy, that the assignment needs to be reviewed, or that in the case of a decay from an isomeric state, the measured short half-life is due to statistical fluctuation.

Theoretically determined spin values of odd-A nuclei discussed before and in the following sections predict angular momenta between 1/2 $\hbar$ and 15/2 $\hbar$ for low energy levels [9,100], so that the considered Δl values are reasonable. However, the measured data are still too sparse for establishing decay schemes. As an example, level schemes predicted in [100] of N – Z = 61 nuclei starting at ^{293}Lv are shown in fig. 11 in [53].

In all cases the chains end by SF resulting in lower limits of b_α values which in turn result in upper limits of HF_α values. For the calculation of the needed WKB half-lives for these nuclei, Q_α values were determined by extrapolation of data shown in fig. 26 in [91]. Upper HF_α limits much less than 1 indicate that the theoretical α energies used for calculation of T_α^{WKB} are low enough so that α decay can be neglected compared to SF. This is the case for ^{265}Rf, ^{277}Hs, and ^{278}Bh nuclei.

Limits of hindrance factors significantly greater than one indicate that the theoretical α energies are too high (the calculated T_α^{WKB} values too low) or that the α decay is significantly hindered. This is the case for ^{283}Cn, N – Z = 59, where fission events observed in an experiment at VASSILISSA were assigned to this nucleus [86,87,89] and for ^{278}Hs, N – Z = 62. However, the decay of both nuclei is not yet confirmed and the assignment of the decay chain terminating at ^{278}Hs is only tentative (see end of sect. 5.1.2).

The four nuclei ^{284}Fl, ^{282}Cn, ^{267}Rf, and ^{284}Cn having HF_α limits closer to one are candidates for a measurable α-decay branch in future experiments. The measurement of α energies of the three even-even nuclei is of particular interest with respect to the determination of binding energies of SHN.

5.1.2 Spontaneous fission half-lives

Theoretical SF half-lives are given in column 9 in table 4. The values are taken from [7,90] for even-even nuclei. In the case of even-odd nuclei, the geometrical mean of the neighboring isotopes was used and for odd-odd nuclei, the geometrical mean of the four neighboring even-even nuclei. Odd particle hindrance factors are not included in the theoretical values. Fission hindrance factors HF_{SF} calculated as ratio of experimental to theoretical half-lives are given in the last column.

In most cases, only upper limits of the SF branchings were measured from which lower limits of hindrance factors result. HF_{SF} limits well below one indicate that the probability for SF of these nuclei is small. HF_{SF} limits near or greater one are not observed for even-even nuclei, except the tentatively assigned nuclei ^{286}Cn and ^{282}Ds (see discussion below). For even-odd nuclei, the greatest limit is $HF_{SF} \geq 14$ for ^{283}Cn. For these nuclei the higher HF_{SF} values can be explained by the odd particle hindering SF.

Six even-even nuclei are available for a comparison between experimental and theoretical SF half-lives. For two of them, ^{294}118 and ^{278}Hs, only a tentative assignment of SF is given. The most reliable data are obtained for ^{284}Fl (HF_{SF} = 0.17), ^{286}Fl (0.23), ^{282}Cn (0.014), and ^{284}Cn (0.029). Values less than one indicate an enhancement of fission relative to the theoretical values. On average, we realize a factor of 5 difference in the case of Fl isotopes and a factor of 50 in the case of Cn. This means that with increasing distance from the predicted region of minimal negative shell-correction energies of spherical SHN the experimental half-lives become increasingly shorter than the predicted ones. The two Cn isotopes are already close to the ridge between the regions of spherical SHN and deformed heavy nuclei around Z = 108 and N = 162, see figs. 1 and 2.

Two reasons could be responsible for theoretically estimating longer SF half-lives. Firstly, the height of the fission barriers (FBE) could decrease more rapidly than assumed departing the region of SHN in south-west direction and, secondly, the width of the fission barriers could become thinner due to a rapider increase of deformation approaching the region of deformed nuclei.

A SF event observed in [82] and assigned to ^{294}118 has a considerably shorter half-life than calculated. An enhancement factor of 10^6 is deduced, which is not understandable on the basis of the presently available data. A classical fission isomer can be excluded due to the high TKE of 223 MeV. Therefore, this event could be a candidate for the decay of an isomer of an isotope of element 118 or a lighter element in the case that a rapid preceding α decay was not detected in the experiment.

In the case of odd-A nuclei, HF_{SF} values can be deduced for eight measured decays. Five of these nuclei (^{265}Rf, ^{283}Cn, ^{279}Ds, ^{271}Sg, ^{281}Ds) have HF_{SF} values between 8 and 100, one (^{277}Hs), for which only one SF event was measured, has $HF_{SF} = 0.5^{+2.2}_{-0.2}$. Four of these nuclei (^{283}Cn, ^{279}Ds, ^{281}Ds, ^{277}Hs) are located in the transitional region between spherical SHN and deformed heavy nuclei and two (^{265}Rf, ^{271}Sg) in the region just below the center of highest stability of the deformed nuclei (see fig. 2). Considering the uncertainties related with the calculation of barrier height and width in these regions, the hindrance factors between 0.5 and 100 are reasonable and within expectations.

This range of measured hindrance factors supports reassignment of a 9.848-MeV α − SF chain measured in [77]

to ^{289}Fl – ^{285}Cn. The HF_{SF} value for ^{285}Cn would be 5.1, and the SF event would be the first observation of a SF branching of this nucleus (see also sect. 4.5).

A relatively high HF_{SF} value of close to 800 is determined for ^{267}Rf. The reason for this could be a high spin value of the ground-state, which results in a high specialization energy [101]. A $13/2^-$ ground-state is predicted for this nucleus, just one neutron above the large level gap at N = 162, whereas a value of $3/2^+$ is predicted for the α-decay parent ^{271}Sg [9].

The assignment of an SF activity observed in early VASILISSA experiments to ^{283}Cn is uncertain [86,87,89]. Nevertheless, a high HF_{SF} value of close to 600 could have a similar reason as discussed before, a high specialization energy of an isomeric state observed in that reactions.

An exceptionally high HF_{SF} value of 7.0×10^5 is obtained for an SF event tentatively assigned to ^{278}Hs of the N – Z = 62 chain. The preceding two α decays of ^{282}Ds and ^{286}Cn, are in good agreement with the expectations. However, the measured half-life of ^{290}Fl is relatively long, see table 4. Therefore, in this special case, one could speculate about possible EC decay of one of these three nuclei which could not be detected in the experiment. This missed EC decay would produce ^{282}Mt, which in turn would α decay into the odd-odd nucleus ^{278}Bh. For this isotope we calculate an unhindered SF half-live of 2.4 ms from the geometrical mean of the theoretical half-lives of the four neighboring even-even nuclei [7,90]. Using the measured half-life of 690 s, an HF_{SF} value of 2.9×10^5 results, which seems to be a reasonable SF hindrance factor for this odd-odd nucleus (see group N − Z = 64 in table 4).

Similar arguments favor the nucleus ^{290}Fl as a most likely candidate for EC decay. Measured SF half-lives of ^{282}Cn (0.96 ms) and ^{284}Cn (118 ms) are factors of 74 and 34, respectively, lower than the theoretical predictions [7]. Consideration of this trend results in a factor of 15 lower SF half-life for ^{286}Cn than the predicted value of 1950 s. The obtained value of 130 s is a factor of 10 smaller than the experimental limit of T_{SF} = 1280 s (640 s/0.5). For that reason it is unlikely that ^{286}Cn is populated by α decay of ^{290}Fl.

In the case of Ds, no fissioning even-even isotopes are known. The partial SF half-life of ^{281}Ds is 14 s, which is shorter than the T_{SF} limit of 134 s of the neighboring even-even ^{282}Ds if this nucleus would be populated. So far, in the region of SHN, the heavier even-even isotope has always a shorter SF half-life than the lighter even-odd neighbor. For those reasons, population of ^{282}Ds in an α-decay chain starting at ^{290}Fl is unlikely too.

Population of ^{278}Hs ($T_{1/2}$ = 690 s) in an α-decay chain of ^{290}Fl would result in the unlikely case that the neighboring odd isotope ^{277}Hs (3.1 ms) has a 2.2×10^5 times shorter SF half-life. Therefore, EC decay of ^{290}Fl to ^{290}113 and population of the odd-odd nucleus ^{278}Bh terminating the chain by SF is most reasonable. Tentatively, this chain is drawn in fig. 2. In that case, this decay chain would be the most neutron-rich decay chain of SHN having an N – Z value of 64. It would be the closest approach to the region of longest half-lives located around N = 182 and Z = 110. The nuclei ^{286}Rg and ^{278}Bh having T_α = 640 s and T_{SF} = 690 s, respectively, would be the longest living SHN known. In addition, it is interesting to note that the measured signals would have been the earliest observation of an α-decay chain starting at an isotope of element 113 although it was not realized in 1999 when the paper [31] was published.

Half-lives for EC are calculated in [9]. According to this prediction, the two nuclei ^{290}Fl and ^{286}Cn are located in the region of nuclei with half-lives greater 100 s, ^{282}Ds should be the most neutron deficient β-stable isotope. However, considering the uncertainties of the calculation, also discussed in [9], half-lives similar or even less than the α half-lives seem to be possible.

Finally, we note that EC of ^{290}114 was already predicted by Fiset and Nix in 1972 [26]. In this theoretical study it was predicted that ^{290}114 will be populated by α decay in a decay chain starting at ^{302}120. In a recent paper, V.I. Zagrebaev, A.V. Karpov, and W. Greiner also investigated the possibility of populating neutron-rich SHN via EC [102].

5.2 Discussion of the signals observed in the reaction ^{54}Cr + ^{248}Cm

Calculated WKB half-lives of the three events measured in the ^{54}Cr + ^{248}Cm reaction result in values of 1.1 μs, 0.16 ms and 18 ms at $\Delta l = 0\,\hbar$, using the measured energies and a tentative assignment to the nuclei ^{299}120, ^{295}118, and ^{291}Lv, respectively. Whereas the third value is in perfect agreement with the known half-life of ^{291}Lv, the second one is a factor of 1130 shorter than the experimental value. For the first event an implanted nucleus could not be unambiguously identified. The closest event having reasonable parameters of an implanted ER, occurred 5.36 s before event α1. In this case a hindrance factor of 3×10^6 results. This unusually large hindrance factor favors the assignment to a chance event. Indeed the background events that could mimic an implanted ER have a mean time interval of 10 s, see sect. 3.2.4.

The first event before α1 was measured 2.26 ms earlier. It was a background event implanted into box-detector segment 11 with an energy of 2.29 MeV having the TOF detector signals in coincidence. This event like all others creates a dead time of 16 μs, so that an implanted ER might be lost. In such a case, the shortest possible lifetime of the first α decay would be 2.26 ms, and a hindrance factor of 1400 would result.

High α-decay hindrance factors of several orders of magnitude are not unusual. Known reasons for high hindrance factors in α decay are spin isomerism (intruder states or Yrast traps and K isomers) or shape isomerism. The heaviest nucleus, where a K isomer was observed, is ^{270}Ds. There, the hindrance factor of a 12.15 MeV α decay is 171, which was explained by a change of angular momentum of $\Delta l = (12 \pm 2)\,\hbar$ [71]. Hindrance factors of 1,800, 15,300, and 13,300 were measured for the α decay of intruder states of the N = 84 nuclei ^{155}Lu, ^{156}Hf and ^{158}W,

respectively [41,103]. All three transitions occur with Δl values of $(10 \pm 2)\,\hbar$.

In order to explain a long half-life of the 13.14-MeV α decay of $^{299}120$ of 1.6 ms or 3.7 s by angular momentum, Δl values of $10\,\hbar$ or $15\,\hbar$, respectively, would be necessary, which would result in half-lives of 1.2 ms and 3.3 s. In the case of the 11.81-MeV α decay of $^{295}118$ a Δl value of $10\,\hbar$ would result in a half-life of 229 ms close to the measured value of 181 ms.

Neutron single-particle levels of high angular momentum are expected by the nuclear shell model for neutron numbers below 184. At oblate shapes, high Ω quasiparticle levels originating from $2h_{11/2}$ $1j_{13/2}$ or $1k_{17/2}$ are located at or near the ground-state, see [9,32,100]. Even higher spin values can be formed for isomers with one or two quasiparticle excitations. Such high spin levels could not only be the reason for high hindrance of α transitions, but also of high hindrance of SF of odd-N isotopes due to a large specialization energy. This latter effect, although not well studied yet, could also significantly reduce the fission probability of the CN and thus result in an increased cross-section, see next sect. 5.3.

Another property of nuclei which could result in high hindrance of α decay is shape isomerism. A theoretical discussion of this phenomenon in the region of SHN is presented in [104] and [105]. Using self-consistent energy density functional theory large oblate level gaps were calculated at Z = 120 and N = 178 and large prolate level gaps at Z = 116 and N = 174 [104]. The region of these proton and neutron numbers overlaps with the nuclei emitting $\alpha 1$, Z = 120, N = 179, and $\alpha 3$, Z = 116, N = 173 and with the emitter of $\alpha 2$, Z = 118, N = 175 as a possibly spherical nucleus between.

Alpha decay of ^{291}Lv populates ^{287}Fl. So far, SF was not observed in that nucleus and a fission branching of $\leq$0.01 is calculated using a theoretical SF half-life, see table 4. As discussed in sect. 4.4, the majority of produced ^{287}Fl nuclei decay with a half-life of 0.54 s into ^{283}Cn. This isotope has a half-life of 4.5 s and a measured SF branching of 0.19. Assuming that the 353 keV event after $\alpha 3$, see table 2, is an escape α emitted from ^{287}Fl, the subsequent SF1 event has too long of a lifetime for an assignment to the well established decay of ^{283}Cn. Lifetime arguments also exclude assigning SF1 to ^{279}Ds, $b_{SF} = 0.85$, in the unlikely case that also the 1.98 MeV event is an escape α.

Most interesting in connection with the events subsequent to $\alpha 3$ are results obtained at the separator VASILISSA at FLNR which were published in 1999 [87,89] and 2004 [86]. Four SF events with long lifetimes were measured in reactions of ^{48}Ca with a ^{238}U target having lifetimes of 3.0, 0.9, 3.0 and 24.3 min [86,87]. Mean values of these results are given in table 4. A mass analysis of the implanted ER resulted in A = 285.1 $\pm$ 4.1 [86] which excludes fission isomers as the origin of the correlated events. The SF events were tentatively assigned to ^{283}Cn.

In order to confirm the first result obtained in [87] using cross-reaction, a ^{242}Pu target was irradiated with ^{48}Ca ions in [89]. Two correlated ER–α–SF chains were measured with lifetimes and energies of 1.32 s, 10.29 MeV and 14.4 s, 2.21 MeV (escape α) for the α decay and 9.3 min and 3.8 min for the correlated SF events, respectively. The two chains were assigned with high probability to the decay of ^{287}Fl.

The mean lifetime of the two α decays is $(7.9^{+14.3}_{-\ 3.1})$ s or $T_{1/2} = (5.4^{+9.9}_{-2.1})$ s and of the six SF events is $(7.4^{+5.1}_{-2.1})$ min or $T_{1/2} = (5.1^{+3.5}_{-1.5})$ min.

Assuming that the 353-keV signal measured subsequent to $\alpha 3$ is an escape α which is together with the SF1 event member of the decay chain, we obtain a lifetime of $(20^{+89}_{-\ 9})$ s for the α decay and of $(12^{+56}_{-\ 5})$ min for the event SF1. The total energy of the escape α is estimated from the lifetime as describe before in the case of ^{283}Cn, see sect. 4.4. An α energy of $(9.53^{+0.09}_{-0.24})$ MeV results, assuming a hindrance factor $HF_\alpha = 1.9$ similar as in the case of 17 known decays of ^{287}Fl, see table 4. The energy with asymmetric error bars is plotted in fig. 9, encircled with a dotted line.

Using an HF_α value of 104 as obtained for the decay of ^{287}Fl from the VASSILISSA experiment, we calculate an energy of $(10.14^{+0.09}_{-0.27})$ MeV from the 20-s lifetime of the 353-keV signal. In this case the energy is in good agreement with the energy of 10.29 MeV measured at VASSILISSA.

Under this aspect, the early Dubna data would support the assignment of the chain measured here, to the decay of $^{299}120$. We remark that the α event of the second chain of ^{287}Fl of the VASSILISSA experiment was also an escape α detected with an energy of 2.31 MeV [89]. For this event a total α energy of $(9.58^{+0.09}_{-0.25})$ MeV is calculated from the lifetime of 14.4 s assuming again a hindrance factor of 1.9 and an energy of $(10.19^{+0.10}_{-0.28})$ MeV assuming a hindrance factor of 104. Both values are in agreement with the total energies calculated for the 353-keV signal of the SHIP experiment.

Later experiments using the reaction ^{48}Ca + ^{238}U at DGFRS [83] and at SHIP [75] for synthesis of isotopes of Cn and the reaction ^{48}Ca + ^{242}Pu at DGFRS [83] for synthesis of Fl did not confirm the results measured at VASSILISSA. So far no attempts were made to explain the early data measured at VASSILISSA. A reason for obtaining different results could be specific properties of the separation method in combination with the de-excitation of short living isomeric states. In addition, different background conditions may hamper the assignment of SF events with long lifetimes.

In conclusion, we realize that existing data and theoretical considerations do not completely contradict the interpretation of the events measured in the ^{54}Cr + ^{248}Cm reaction as being due to a decay chain starting at $^{299}120$ and terminating at ^{283}Cn. However, we also have to admit that theoretical arguments must be applied for which no experimental evidence is given so far and that experimental results are used which themselves are not yet confirmed. On the other hand, a partial agreement with proven experimental data (α decay of ^{291}Lv) and the low probability of the event chain for emerging by chance are arguments for possible production of element 120. In the

subsequent section, we examine the reaction cross-section for further support or arguments for disproof.

5.3 Shell-correction energies, fission barriers, and cross-section

In models commonly used in calculations of ER cross-sections in fusion reactions of heavy ions it is assumed that after capture of the reacting nuclei a CN nucleus is formed at a certain excitation energy, E*, which then cools down by evaporation of neutrons and γ rays. In fusion of SHN, the ER cross-section is highly reduced, firstly, due to re-separation of the nuclei by the so called quasi-fission in the entrance channel and, secondly, by the high probability of fission of the CN. Both quantities are not well known, because in experiments it is often difficult to distinguish between fragments of the two reaction types, both being emitted with high energies. Nevertheless, measured ER cross-sections of reactions with a ^{48}Ca beam and actinide targets are reproduced or were predicted rather well, see *e.g.* [47] for a comparison of experimental and calculated cross-sections. Refined cross-section calculations as described *e.g.* in [61,106–110] take these processes into account, which depend on charge, size, and deformation of projectile and target nuclei, damping of shell effects which reduces FBE [111–113] as function of E*, level densities, angular momenta, and neutron binding energies.

However, the cross-section predictions for synthesis of element 120 cover a wide range from 0.07 to 8000 fb depending on the model and the FBE used. Reactions with beams of ^{50}Ti, ^{54}Cr, and ^{58}Fe and targets of ^{249}Cf, ^{248}Cm, and ^{244}Pu, respectively, were investigated in the calculations. The cross-section measured in this work for the three event chain observed in the reaction ^{54}Cr + ^{248}Cm tentatively assigned to ^{299}120 is $(0.58^{+1.34}_{-0.48})$ pb.

An important component hampering the cross-section calculations is the lack of knowledge of the fission barrier and its attenuation at high excitation energy. Theoretical estimates reveal how sensitively the cross-sections depend on FBE. In [106], the cross-section changed by a factor of 200 for the ^{48}Ca + ^{249}Cf reaction when an FBE of ≈5.5 MeV [114] was changed by ±1 MeV. In [115,116], the 3n cross-section of the ^{48}Ca + ^{238}U reaction was calculated for FBE of 4.5, 5.5, and 6.5 MeV resulting in cross-sections of 0.23, 5.0, and 30 pb, respectively. That calculation reveals that a decrease of the FBE is more sensitive than an increase, which is a result of the exponential dependence of the cross-section on the FBE.

Experimental data on FBE of SHN do not exist. The heaviest nucleus from which FBE was deduced, is the deformed ^{254}No. The data were derived at the fragment mass analyzer (FMA) at Argonne National Laboratory [117]. An FBE of (6.0 ± 0.5) MeV was measured at spin 15 $\hbar$ from which a value of (6.6 ± 0.9) MeV was extrapolated for spin 0 $\hbar$. In this case identical predictions of the FBE = 6.76 MeV were obtained in [118] and [119] which agree well with the measured value.

In order to better estimate the uncertainty of model predictions, we used the measured Q_α values for deter-

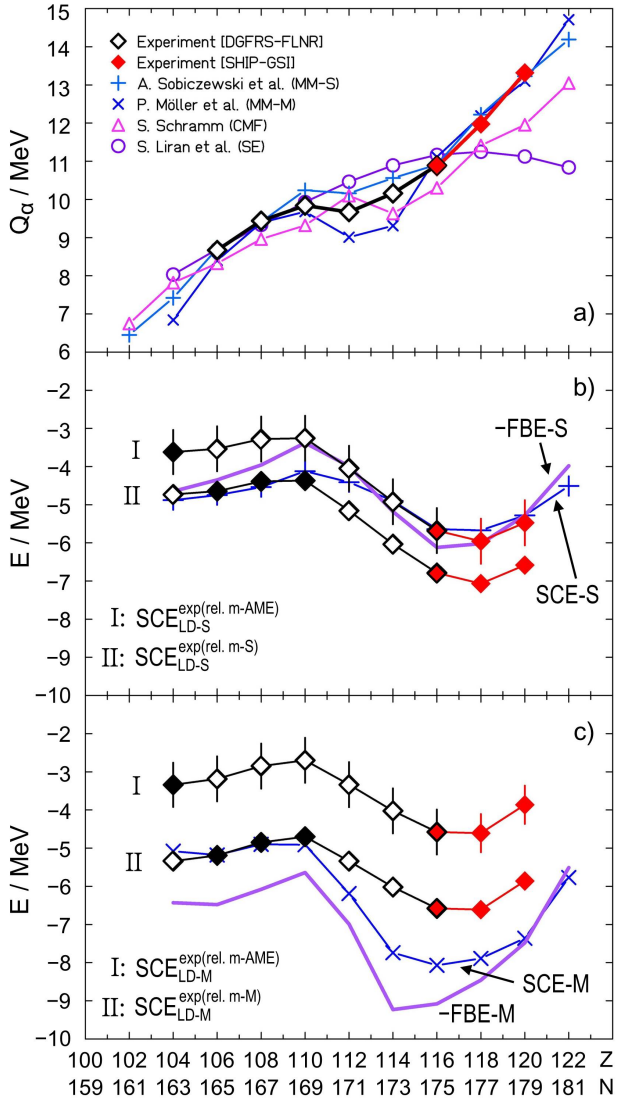

Fig. 10. Comparison of experimental and theoretical Q_α values for nuclei of the α-decay chain passing through the isotope ^{291}Lv (a). Experimental Q_α values of nuclei from ^{271}Sg to ^{291}Lv were taken from [57]. Theoretical Q_α values were taken from the macroscopic-microscopic models by A. Sobiczewski *et al.* [54,55,114] (MM-S) and P. Möller *et al.* [97] (MM-M), the chiral mean-field model (CMF) by S. Schramm [37], and a semi-empirical model (SE) by S. Liran *et al.* [99]. Experimental shell-correction energies of the decay chain are compared with theoretical values of the MM-S model in (b) and of the MM-M model in (c). Experimental data with error bars are based on the AME masses, from which the theoretical LD masses, LD-S and LD-M, were subtracted. Experimental data without error bars are based on the theoretical masses. They better reflect different trends between experiment and theory along the measured decay chains. In (b,c) these masses were fitted to the theoretical masses of ^{271}Sg, ^{275}Hs and ^{279}Ds. Note that within an α-decay chain the shape of the experimental SCE curves is fixed by the measured Q_α values and the used theoretical LD masses. Curves without symbols show the negative values of the heights of the fission barriers, –FBE-S and –FBE-M, obtained in models MM-S and MM-M.

mining relative masses of SHN along α-decay chains. All measured decay chains of even elements were investigated. These have N – Z values of 57, 58, 59, 60, and 61 The chains start at ^{285}Fl, ^{294}118, ^{291}Lv, ^{292}Lv, and ^{293}Lv. The results were published in [120] where the data evaluation is described in detail. From that work we took the data of the N – Z = 59 chain and extend it by the new values tentatively assigned to ^{299}120 and ^{295}118.

As outlined in [120], none of the chains end in a nucleus with known mass. Therefore, the relative masses of nuclei at the end of the chains were normalized to the theoretically predicted masses and, as a second option, to the mass estimates given in the AME2012 evaluation [91,121]. The so determined partial, but model dependent 'experimental data' were compared with the results of the MM calculations of Sobiczewski *et al.* [54,55] (MM-S) and Möller *et al.* [9] (MM-M). Information on the shell-correction energy (SCE) was deduced by subtracting the theoretical liquid-drop (LD) masses, which differ in the two models, from the experimental masses.

In the region of SHN, the FBE is predominantly determined by ground-state SCE, because the LD fission barrier vanishes at about Rf and at the saddle point the SCE are assumed to be small [122]. Therefore, negative values of SCE are often used as FBE for determining the fission probability of CN in cross-section calculations. This was always the case when calculated values of the FBE were not available.

The mutual dependence becomes obvious in a comparison of the SCE with the negative values of the FBE. We compare in figs. 10b and c the calculated FBE in the MM-S and MM-M model with experimental and theoretical SCE values. In both FBE calculations, a specialization energy which increases the FBE due to energy shifts of the odd neutron at deformation during the fission process, is not considered.

The curves of SCE and –FBE in fig. 10 reveal a good agreement between experiment and theory in the case of the MM-S model, whereas the MM-M model predicts too strong of an SCE in the region of Fl and Sg. As a result the corresponding Q_α values plotted in fig. 10a are too low in the MM-M model. However, both models and the experimental data agree with an increase of the curves for nuclei beyond Lv resulting in less stability and lower FBE for the heavier nuclei. In particular, a reduction of Q_α values due to the influence of a shell or subshell at Z = 120 is not observed at N $\approx$ 179.

Important for an estimate of the ER cross-section of element 120 is the change of the FBE (here we use the negative of SCE instead) from Z = 114 towards the heavier elements. The calculated values of the two models, MM-S and MM-M, are plotted as function of the neutron number in fig. 11. Included are the model dependent experimental data based on the AME-2012 mass evaluation [91,121]. The figure was taken from [120] but amended by the two values deduced from the decay of the nuclei tentatively assigned to ^{299}120 and ^{295}118.

We observe good agreement for all studied nuclei in the case of the MM-S model, fig. 11a. However, the strong shell

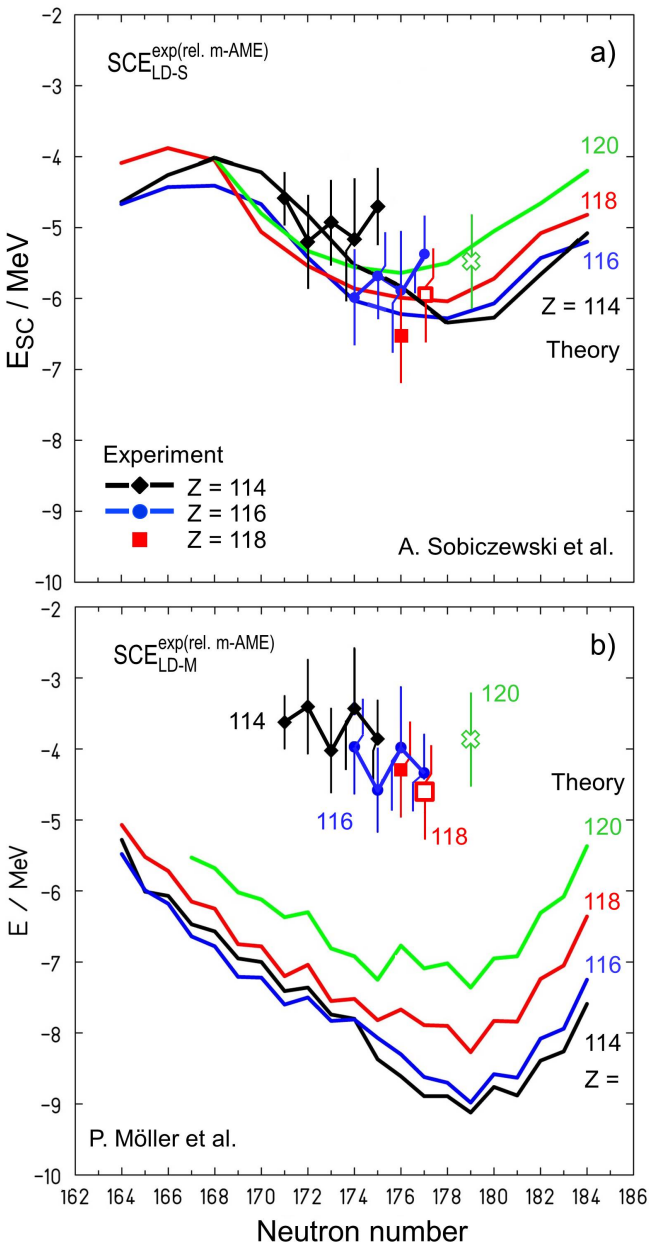

Fig. 11. Model dependent experimental shell-correction energies of isotopes of elements flerovium, livermorium and 118 (filled symbols) and of the values deduced from the decays of nuclei tentatively assigned to ^{295}118 and ^{299}120 (open symbols, crosses for Z = 120) are compared with theoretical predictions of the MM-S model in (a) and of the MM-M model in (b). In (a) theoretical values of only the even-even nuclei are plotted. The difference between experimental data in (a) and (b) is due to differences of the LD masses of the two models MM-S and MM-M. The experimental SCE values with error bars are based on the mass estimates of the AME-2012 mass evaluation [91,121]. The figure is a modified version of fig. 4 in [120].

effects calculated in the MM-M model in particular for isotopes of Fl and Lv at neutron numbers of about 178 are not observed in the experimental data. The values differ by about 4 MeV. A difference of about 1 – 2 MeV between experimental data in (a) and (b) is due to different LD masses of the models.

At a first glance it seems contradictory that lower fission barriers should result in higher cross-sections for production of element 120. However, as outlined in [120], the low fission probability of the CN of Fl and Lv due to high FBE is compensated by a higher probability of quasi-fission in the entrance channel in order to reproduce the measured cross-sections. If in reality, the FBE is less for Fl and Lv, then quasi-fission must be less, too.

In fig. 11, we see that the SCE values of $^{299}120$ are similar to those of Fl and Lv and not about 2 MeV less as calculated in MM-M. Therefore, cross-section calculations which use –SCE of the MM-M model as an estimate for the fission barrier of Z = 120 isotopes will obtain cross-sections that are too low. A cross-section of 28 fb was predicted for the reaction ^{248}Cm(^{54}Cr,4n)$^{298}120$ in [61]. A rough estimate based on the arguments given before, but considering the higher quasi-fission probability due to the less asymmetric reaction with a ^{54}Cr beam, reveals that the cross-section could be a factor of 4 to 20 higher, which means 0.1 – 0.5 pb [120]. The cross-section measured in this work was $(0.58^{+1.34}_{-0.48})$ pb.

Also, the systematics of maximum cross-section as function of E* for various reactions using a ^{248}Cm target was studied in [120]. The data were compared with calculated values for reactions at beam energies just high enough to reach a contact configuration according to the fusion model of [123].

In this case, the maxima of measured cross-sections for synthesis of isotopes of No up to Hs are about 3 MeV above the calculation for beams of neutron rich isotopes of carbon, oxygen, neon, magnesium and 7 MeV for ^{48}Ca for synthesis of Lv. In this latter reaction, a local minimum of the excitation energy occurs due to the strong binding of the double magic ^{48}Ca, see fig. 5 in [120]. For the ^{54}Cr + ^{248}Cm reaction, the contact configuration results in E* = 31 MeV. However, the irradiation was performed at E* = 42 MeV, which was estimated from systematics of measured and calculated excitation functions of hot fusion reactions. It seems possible that this value is 4 MeV too high compared with the optimum case for the reaction with ^{48}Ca beam.

In recent publications, the FBE values are explicitly given; these are based on the MM-S model in [118] and on the MM-M model in [119,124]. For comparison with ground-state SCE, the negative values, –FBE-S and –FBE-M are plotted in figs. 10a and b, respectively. Only small differences between –FBE-S and SCE-S exist in the region of SHN, whereas the differences between –FBE-M and SCE-M are about 1 MeV for ^{287}Fl and ^{291}Lv. The same relationships were also observed for the neighboring nuclei with N – Z values from 57 to 61, see fig. 3 in [120]. Obviously, the increase of the fission barrier relative to the negative of ground-state shell-correction energy is due to a pronounced positive saddle-point shell-correction energy in the MM-M model [119,124]. Consequently, cross-section calculations for synthesis of Fl and Lv using the higher FBE-M values need a higher quasi-fission probability (due to less fission of the CN), in order to reproduce the measured values.

However, the difference between FBE-M and –SCE-M vanishes at $^{299}120$. Therefore, the faster decrease of the fission barrier (compared to the previously used –SCE values as barrier) will result in reduced ER cross-sections, when the higher quasi-fission probability is kept.

From α-decay Q values, we get information only on the ground-state SCE. However, the results from this study revealed such a big difference between the experimental SCE and the SCE-M values, that a possible positive saddle-point shell-correction energy of about 1 MeV will not significantly change the qualitative arguments related to the prediction of the cross-section for synthesis of element 120.

Finally, it should be mentioned that an increase or a decrease in the damping of shell-correction energies at high excitation energies will also increase or decrease the fission of the CN, respectively. An increase of CN fission by this effect demands less quasi-fission in the entrance channel and *vice versa* in order to reproduce measured cross-sections when the ground-state fission barrier is fixed.

6 Summary and outlook

We investigated the reaction ^{54}Cr + ^{248}Cm in an attempt to produce the new element 120. At an excitation energy of 42 MeV of the compound nucleus $^{302}120$, we expected emission of three neutrons and thus production of the isotope $^{299}120$. Three correlated α-decay like signals denoted as α1, α2, and α3, and an also correlated SF event were observed. The probability is low that this chain of signals is produced by chance. The energies of the three signals coincide with predictions of macroscopic-microscopic models for α decay of the nuclei $^{299}120$, $^{295}118$, and ^{291}Lv. However, an implanted nucleus starting the decay chain could not be identified unambiguously. It could have been missed due to deadtime in the focal plane detector or its lifetime is significantly longer than expected from an unhindered α decay of an isotope of element 120 at the measured decay energy. The lifetime of the potential daughter nucleus, $^{295}118$, is also one thousand times longer than expected. However, the lifetime and energy of the third signal is fully in agreement with previously measured α-decay data of ^{291}Lv.

A low probability for emerging by chance was determined for an also measured high energy signal which occurred 12 min after α3. Also, in this case the lifetime is significantly longer than measured and accepted data of decay products ^{287}Fl, ^{283}Cn, or ^{279}Ds. However, this potential SF event and a low energy signal 20 s following α3, which could be an escape α, agree well with former data measured at the separator VASSILISSA at FLNR, which were assigned to α decay of ^{287}Fl and SF of ^{283}Cn [86,87, 89]. These data were not confirmed in later experiments,

but also not disproved and a different assignment is not yet given.

Due to this uncertainty, and the problems with the assignment of our observations from the irradiation of ^{248}Cm with ^{54}Cr ions, we reviewed the measured data on even SHN obtained since 1998. A few data could be corrected including one decay chain measured in our previous study of the reaction ^{48}Ca + ^{248}Cm, which was tentatively assigned to isomeric decays in the decay chain of ^{293}Lv in [53], which, however, is now more reasonably assigned to the decay chain of ^{291}Lv produced in a reaction with the 3.1 % target contamination of ^{246}Cm.

A comparison of the experimental data with results of the MM models of Sobiczewski *et al.* and Möller *et al.* reveals a rather good agreement concerning properties of α decay and SF. In particular, the much higher probability for α decay compared to SF of nuclei in the island of SHN is verified.

However, from a detailed analysis of measured Q_α values aiming to extract shell-correction energies and related fission barriers, we deduced a lower fission barrier for Fl and Lv isotopes than predicted by Möller *et al.* who calculate particularly high fission barriers for these isotopes. The results of this study and consequences for cross-section calculations were published in a separate paper [120].

During periods with slightly higher energy contamination of the beam, we observed as a by-product a number of nuclei possibly up to fermium, which were produced by multi-nucleon transfer reactions. This result shows that separators like SHIP are well suited to study such reactions at beam energies at and below the classical fusion barrier, when a considerable fraction of the reaction products are emitted in forward direction. Recent results including production of new isotopes of heavy elements via multi-nucleon transfer are published in [125,126]. In these experiments the velocity separation of the filter were tuned for separation of such transfer products.

We are aware that the three correlated events observed in the ^{54}Cr + ^{248}Cm reaction cannot be assigned definitely. The possibility that one or more signals discussed here are not radioactive decays, but background events, cannot be completely excluded. However, the analysis of the experiment, the review of the existing data, and in particular the elaboration of fission barriers and related cross-sections, suggests that the cross-section for synthesis of element 120 could be higher than previously expected. A consequence of our result, if confirmed in future experiments, would be that shell effects decrease beyond element 116 but less rapidly as predicted by the MM model of Möller *et al.*. This observation might be caused by a not negligible effect of the closure of a subshell at element 120 and a low level density extending up to Z = 126.

Due to the lack of beam time, we could not continue the irradiations at SHIP aiming to confirm the observation made in a relatively short first part of the total of 140 days of beam time requested for this experiment. Meanwhile it is certain that this experiment can not be continued at SHIP. Therefore, we believe that it is justified to publish the data as they were measured in 2011.

The results including those of the review may be of interest for search experiments for element 120 being in preparation at other laboratories. At DGFRS in Dubna a target of ^{249}Cf (50.4 %), ^{250}Cf (13.5 %), and ^{251}Cf (36.1 %) is presently irradiated with a ^{48}Ca beam. In this experiment heavier isotopes than the known ^{294}118 will be produced. The results will also show if the cross-section will increase when heavier target isotopes are used and the CN are closer to the center of strongest SCE, see figs. 1 and 2. In a second step, it is planned to switch the beam from ^{48}Ca to ^{50}Ti for synthesis of element 120 [73,127]. The target of mixed isotopes has to be used because highly enriched material of ^{250}Cf and ^{251}Cf is not available and the specific activity of ^{252}Cf is too high. Such a target wheel can be handled only under extreme safety conditions.

At GARIS at RIKEN, it is planned to produce isotopes of element 118 using the reaction ^{50}Ti + ^{248}Cm $\rightarrow$ ^{298}118* and in a second step to switch the beam to ^{54}Cr for synthesis of element 120 as in our experiment at SHIP [128,129].

The progress towards the exploration of the island of SHN is difficult to predict. Hot fusion based on actinide targets and ^{48}Ca beams terminate at element 118, because targets beyond Cf can be produced only with tremendous costs and efforts. How heavier beams like ^{50}Ti, ^{54}Cr, *etc.* will affect the fusion cross-section is subject of experiments planned for the near future. However, these heavier beams are mandatory for exploration of the island of SHN into the north-east direction, the direction towards new elements. Strong shell effects, if they exist at Z = 120 or 126, could positively influence the reaction cross-sections. Alpha energies measured of more isotopes of element 118 and of the new element 120 may already help to settle this uncertainty.

In this context, it is worthwhile to study the transition from high to low excitation energies, namely from hot to cold fusion, which is expected to occur with actinide targets and the strongly bound isotopes of iron and nickel for synthesis of elements on the way to Z = 126. Increased losses by re-separation in the entrance channel due to the higher Coulomb repulsion could possibly be compensated by a lower probability of CN fission.

No technical limitations exist for exploration of the island of SHN towards the west. Sufficient neutron deficient projectile isotopes are available. However, due to Q-value effects the excitation energy of the CN at barrier energies will increase.

Most interesting, but also most difficult, will be the synthesis of more neutron-rich isotopes located in the south-east direction of the island of SHN. There, the longest half-lives are expected. Reactions using radioactive beams and multi-nucleon transfer reactions are options to be studied in the future. Searching for electron capture decay branches could be another option. An example, as discussed in this paper, could be electron capture of ^{290}Fl populating an α-decay chain starting at ^{290}113 and terminating by SF of ^{278}Bh.

Using transfer reactions as suggested in [130], low beam energies and hence observation in the zero degree direc-

tion are mandatory, in order to produce the fragments at the lowest possible excitation energy and thus reduce fission, in particular of the heavy, high Z fragment. Systems as heavy as ^{238}U + ^{248}Cm are technically possible and could be investigated with a modern separator and detection methods. These methods will also allow for measuring contact times of dinuclear systems by making use of the kinematics of the reaction products at the moment of re-separation after rotation of the system at small impact parameters [131].

Excitation functions have to be measured, which provide information on how fast the cross-section decreases with increasing energy due to fission of the CN, and how fast cross-sections decrease on the low energy side due to the fusion barrier and re-separation of projectile and target nuclei. From both slopes, information about the shape of the fission and the fusion barriers can be obtained. The study of transfer products may open a direct access to the first steps of the processes resulting in fusion. Due to the low beam energy the reactions occur in central collisions and the reaction partners re-separate in and opposite to the beam direction. Therefore velocity separators like SHIP are an ideal tool to study these processes.

The classical cold fusion reactions based on lead and bismuth targets will be further used for exploring the regions of increased stability of deformed heavy nuclei located around Z = 108, N = 162 and Z = 100, N = 152. How far these regions extend into the west and north-west direction is a question which has to be answered. Also, whether SF or proton emission will determine the limits.

Element 114 was discovered in a hot fusion reaction. However, another possibility could be the cold fusion reaction ^{76}Ge + ^{208}Pb. As predicted by the late Władysław Świątecki using his fusion-by-diffusion model [132], the cross-section should be considerably higher than the one for synthesis of element 113. This experiment is still waiting to be performed.

At high enough cross-sections, the measurements can be complemented by in-beam γ-ray spectroscopy using recoil-decay tagging methods in order to study the influence of angular momentum on the fusion and survival probability. Observation of characteristic X rays emitted during the de-excitation cascade could help identifying the produced nuclei.

A comparison of experimental and theoretical SF half-lives of the known even-even isotopes of Ds and Fl is difficult, because these nuclei are located in a transitional region between spherical SHN and deformed heavy nuclei and the degree of deformation is not known. The measurement of small SF branchings of more neutron rich even isotopes of Fl, which are located closer to the center of the island of spherical SHN, will allow for a solid comparison of experimental and theoretical SF half-lives. Expected are significant data on fission barriers of spherical SHN, which are needed for better estimates of production cross-sections in various reactions as *e.g.* fusion with radioactive neutron rich beams, multi-nucleon transfer reactions and rapid neutron capture in a stellar environment. The latter aspect is closely related to the question, if SHN could be produced in nature and how long they could survive.

Important for determination of masses of nuclei along α-decay chains is the detection of small α-decay branchings, in particular of neutron-rich even-even isotopes of Ds, which decay dominantly by SF, and α decay was not yet observed.

Also important are measurements of masses of nuclei at the end of the α-decay chains. Their half-lives are long so that ion traps or multi-reflection time-of-flight mass spectrometers can be used. These neutron rich nuclei being located in the region of elements from Rf to Sg are presently produced at low cross-section as decay products of SHN. However, in future experiments with radioactive beams or in multi-nucleon transfer reactions these nuclei could be directly produced with higher yield. The mass measurements of No and Lr isotopes with SHIPTRAP represent a major breakthrough in Penning trap mass spectrometry.

Stopping of the separated reaction products in gas catchers and injection of the low energy beam in penning-trap or multi-reflection TOF spectrometers will allow for isobaric purification, accurate mass determination and precise decay spectroscopy. Compared to present techniques, the long half-lives expected for some of the neutron-rich SHN, are not a limitation, but on the contrary, the precision increases with increasing half-life. In addition, atomic beam experiments as *e.g.* collinear laser spectroscopy and Stern-Gerlach experiments will also become possible. In the near future, further technical improvements such as a cryogenic stopping cell, will be implemented, a major step into direction of higher sensitivity.

The region far beyond element 126 was already addressed theoretically 40 years ago. For example, a region of relatively higher stability against SF was predicted at Z = 164 and N = 318 in [25]. Although such heavy nuclei may not exist, the shell structure could influence the lifetime of an intermediate resonance like structure.

The properties of toroidal and spherical bubble nuclei were presented in [133,134]. Although speculative, the highly advanced experimental technology should be used also for some experiments to search for such really exotic phenomena in this region of nuclei, which is accessible using the heaviest beams and targets.

Accelerators, separators, detectors, signal processing, and data acquisition presently in use are highly developed and should be used for the continuation of experiments. However, improvements are still possible. The most powerful dedicated facility under construction will be the 'SHE Factory' at FLNR in Dubna delivering beam intensities of up to 10 particle μA. The GANIL laboratory in France will open new facilities to study SHN. The new Facility for Radioactive Ion Beams (FRIB), under development at Michigan State University, intends to use RIBs to study more neutron-rich SHN. AT GSI a new accelerator dedicated to SHN research was already suggested in 1999 [135]. The advantages of a superconducting CW (continuous wave) linear accelerator were worked out in 2004 and presented in [136,137]. In addition to a factor of three less

power consumption the beam intensity could be increased by a factor of 3.8 even without further improvement of the beam from the ion source, compared to the performance of the present UNILAC.

New and more precise experimental data will again trigger theoretical studies. So, one can hope that still existing uncertainties related with the stability of SHN and the various reactions for producing them will eventually be solved.

7 Dedication and acknowledgments

We dedicate this paper to our teacher, colleague, and friend Walter Greiner who celebrated his 80th birthday on October 29th, 2015. Walter Greiner has initated and developed the theoretical understanding of a wide range of phenomena in nuclear physics, nuclear reactions, and strong quantum fields. He is one of the fathers of our laboratory, the Gesellschaft für Schwerionenforschung (GSI) founded in 1969 for basic research in heavy ion physics. In our field, the research in super-heavy nuclei, this farsighted initiative led to the discovery of the new elements from bohrium (Z = 107) to copernicium (112) and to the development of separation and detection techniques which were adopted in other laboratories where new super-heavy nuclei were synthesized up to the presently heaviest known nucleus with atomic number 118.

The study of these super-heavy nuclei is one of the great interests of Walter Greiner, which he considered as one of the important research fields to be investigated in nuclear physics, atomic physics, and chemistry. In particular, as director of the Institute for Theoretical Physics at Goethe University Frankfurt and since 2003 as founding director of the Frankfurt Institute for Advanced Studies (FIAS) his ideas of 'cold fusion valleys' and fragmentation theory have driven successful experimental search for these super-heavy nuclei. We are particularly grateful to Walter Greiner for his readiness to listen and to give advice whenever we asked.

For the future we wish Walter Greiner quick recovery from his illness so that we can continue discussions with him and that he can participate in the results of new experiments which will be obtained at GSI and collaborating laboratories in the field of super-heavy nuclei.

We gratefully acknowledge stimulating discussions with Valeriy Zagrebaev who unexpectedly passed away in January 2015. We thank Peter Möller and Adam Sobiczewski for elevated guidance and supplying us with results of calculations prior to publication. Delightful discussions with Gurgen G. Adamian, Nikolai V. Antonenko, Vitali Denisov, Joachim Maruhn, Avazbek Nasirov are gratefully acknowledged.

The implementation of experiments at SHIP was only possible due to considerable support from various departments of GSI. In particular we thank the scientist and technicians of the UNILAC accelerator, the target laboratory, computing center, and the people in the administration. We also take the opportunity to thank our colleagues working at the collaborating laboratories. The intense and long lasting cooperation with FLNL, its scientific leader Yuri Ts. Oganessian and the directors Sergey N. Dmitiriev and Mikhail G. Itkis is especially acknowledged. Close connections existed to the laboratories JYFL, LLNL, ORNL, RIKEN, and last not least various industrial companies. We are obliged to all of them. S. Hofmann thanks the Helmholtz Association for the award of a Helmholtz Professorship and the GSI administration for support after retirement.

Work at LLNL was performed under the auspices of the U.S. Department of Energy by Lawrence Livermore National Laboratory under Contract DE-AC52-07NA27344. S. Antalic acknowledges support from the Slovak grant agency VEGA (contract No. 1/0576/13) and the Slovak Research and Development Agency (contract No. APVV-0105-10).

References

1. O. Hahn and F. Straßmann, Naturwissenschaften **27**, 11 (1939).
2. L. Meitner and O.R. Frisch, Nature **143**, 239 (1939).
3. G.N. Flerov and K.A. Petrjak, Phys. Rev. **58**, 89 (1940).
4. G.T. Seaborg and W.D. Loveland, *The elements beyond uranium*, John Wiley and Sons, Inc., New York, 1990, pp. 1-359
5. J.A. Wheeler, *Niels Bohr and the Development of Physics*, Pergamon Press, pp. 163–184 (1955).
6. J.A. Wheeler, *Proc. Int. Conf. on the Peaceful Uses of Atomic Energy, Volume 2*, United Nations, New York, pp. 155–163 (1955).
7. R. Smolanczuk, J. Skalski, A. Sobiczewski, Phys. Rev. C **52**, 1871 (1995).
8. R. Smolanczuk, A. Sobiczewski, *Shell effects in the properties of heavy and superheavy nuclei*, Proc. XV. Nuclear Physics Divisional Conference on Low Energy Nuclear Dynamics, Yu.Ts. Oganessian, R. Kalpakchieva, W. von Oertzen, eds., St.Petersburg, Russia, 1995, World Scientific, Singapore, p. 313 (1995).
9. P. Möller, J.R. Nix, K.L. Kratz, At. Data Nucl. Data Tables **66**, 131 (1997).
10. G. Soff, J. Rafelski, W. Greiner, Phys. Rev. A **7**, 903 (1973).
11. J. Reinhardt, B. Müller, W. Greiner, Phys. Rev. A **24**, 103 (1981).
12. C. Kozhuharov, P. Kienle, E. Berdermann, H. Bokemeyer, J. S. Greenberg, Y. Nakayama, P. Vincent, H. Backe, L. Handschug, E. Kankeleit, Phys. Rev. Lett. **42**, 376 (1979).
13. M. Göppert-Mayer, Phys. Rev. **74**, 235 (1948).
14. O. Haxel, J.H.D. Jensen, H.E. Suess, Die Naturwissenschaften **36**, 376 (1949).
15. V.M. Strutinsky, Nucl. Phys. A **95**, 420 (1967).
16. S.M.Polikanov, V.A.Druin, V.A.Karnaukov, V.L.Mikheev, A.A. Pleve, N.K. Skobolev, V.G.Subotin, G.M.Ter-Akopian, V.A.Fomichev, Sov. Phys. JETP **15**, 1016 (1962).
17. Yu.Ts. Oganessian, A.G. Demin, A.S. Iljinov, S.P. Tretyakova, A.A. Pleve, Yu.E. Penionzhkevich, M.P. Ivanov, Yu.P. Tretyakov, Nucl. Phys. A **239**, 157 (1975).
18. S.G. Nilsson, C.F. Tsang, A. Sobiczewski, Z. Szymanski, S. Wycech, C. Gustafson, I.L. Lamm, P. Möller, B. Nilsson, Nucl. Phys. A **131**, 1 (1969).

19. W.D. Myers, W.J. Świątecki, Nucl. Phys., **81**, 1 (1966).
20. A. Sobiczewski, F.A. Gareev, B.N. Kalinkin, Phys. Lett. **22**, 500 (1966).
21. H. Meldner, Ark. Fys. **36**, 593 (1967).
22. S.G. Nilsson, J.R. Nix, A. Sobiczewski, Z. Szymanski, S. Wycech, C. Gustafson, P Möller, Nucl. Phys. A **115**, 545 (1968).
23. S.G. Nilsson, S.G. Thompson, C.F. Tsang, Phys. Lett. B **28**, 458 (1969).
24. U. Mosel, W. Greiner, Z. Phys. **222**, 261 (1969).
25. J. Grumann, U. Mosel, B. Fink, W. Greiner, Z. Phys. **228**, 371 (1969).
26. E.O. Fiset, J.R. Nix, Nucl. Phys. A, **193**, 647 (1972).
27. J. Randrup, S.E. Larsson, P. Möller, S.G. Nilsson, K. Pomorski, A. Sobiczewski, Phys. Rev. C **13**, 229 (1976).
28. W. Grimm, G. Herrmann, H.-D. Schüssler, Phys. Rev. Lett. **26**, 1040 (1971).
29. G.N. Flerov, G.M. Ter-Akopian, Rep. Prog. Phys. **46**, 817 (1983).
30. G.M. Ter-Akopian, S.N. Dmitriev, Nucl. Phys. A **944**, 177 (2015).
31. Yu.Ts. Oganessian, V.K. Utyonkov, Yu.V. Lobanov, F.Sh. Abdullin, A.N. Polyakov, I.V. Shirokovsky, Yu.S. Tsyganov, G.G. Gulbekian, S.L. Bogomolov, B.N. Gikal, *et al.*, Phys. Rev. Lett. **83**, 3154, (1999).
32. S. Ćwiok, J. Dobaczewski, P.H. Heenen, P. Magierski, W. Nazarewicz, Nucl. Phys. A, **611**, 211 (1996).
33. K. Rutz, M. Bender, T. Bürvenich, T. Schilling, P.G. Reinhard, J.A. Maruhn, W. Greiner, Phys. Rev. C **56**, 238 (1997).
34. A.T. Kruppa, A.T. Kruppa, M. Bender, W. Nazarewicz, P.G. Reinhard, T. Vertse, S. Ćwiok, Phys. Rev. **C61**, 034313 (2000).
35. M. Bender, W. Nazarewicz, P.G. Reinhard, Phys. Lett. B **515**, 42 (2001).
36. M. Bender, P. Bonche, T. Duguet, P.H. Heenen, Nucl. Phys. A **723**, 354 (2003).
37. S. Schramm, Phys. Rev. C **66**, 064310 (2002) and private communication (2014).
38. S. Mişicu, T. Bürvenich, W. Greiner, J. Phys. G: Nucl. Part. Phys. **28**, 1441 (2002).
39. D.C. Hoffman, Nucl. Phys., A **502**, 21c (1989).
40. G. Münzenberg, W. Faust, S. Hofmann, P. Armbruster, K. Güttner, H. Ewald, Nucl. Instrum. Methods **161**, 65 (1979).
41. S. Hofmann, W. Faust, G. Münzenberg, W. Reisdorf, P. Armbruster, K. Güttner, H. Ewald, Z. Phys. A **291**, 53 (1979).
42. S. Hofmann, G. Münzenberg, Rev. Mod. Phys. **72**, 733 (2000).
43. K.H. Schmidt, R.S. Simon, J.G. Keller, F.P. Heßberger, G. Münzenberg, B. Quint, H.G. Clerc, W. Schwab, U. Gollerthan, C.C. Sahm, Phys. Lett. B **168**, 39 (1986).
44. G. Münzenberg, *In-flight separation of heavy ion beams in Experimental Techniques in Nuclear Physics*; Poenaru, D.N and Greiner, W., Eds., Walter de Gruyter, Berlin - New York, 1997, p. 375-424
45. S. Hofmann, Rep. Prog. Phys. **61**, 639 (1998).
46. K.E. Gregorich, Nucl. Instrum. Methods Phys. Res., Sect. A **711**, 47 (2013).
47. Yu.Ts. Oganessian, V.K. Utyonkov, Rep. Prog. Phys. **78**, 036301 (2015).
48. K. Morita, Nucl. Phys. A **944**, 30 (2015).
49. Yu.Ts. Oganessian, V.K. Utyonkov, Yu.V. Lobanov, F.Sh. Abdullin, A.N. Polyakov, R.N. Sagaidak, I.V. Shirokovsky, Yu.S. Tsyganov, A.A. Voinov, A.N. Mezentsev *et al.*, Phys. Rev. C **79**, 024603 (2009).
50. S. Hofmann, D. Ackermann, S. Antalic, V.F. Comas, S. Heinz, J.A. Heredia, F.P. Heßberger, J. Khuyagbaatar, B. Kindler, I. Kojouharov *et al.*, *GSI Scientific Report 2008,* GSI Report **2009-1**, 131 (2009).
51. J. Khuyagbaatar, A. Yakushev, Ch.E. Düllmann, H. Nitsche, J. Roberto, D. Ackermann, L.-L. Andersson, M. Asai, H. Brand, M. Block *et al.*, *GSI Scientific Report 2012*, GSI Report **2013-1**, 131 (2013).
52. J.B. Roberto, C.W. Alexander, R.A. Boll, J.D. Burns, J.G. Ezold, L.K. Felker, S.L. Hogle, K.P. Rykaczewski, Nucl. Phys. A **944**, 99 (2015).
53. S. Hofmann, S. Heinz, R. Mann, J. Maurer, J. Khuyagbaatar, D. Ackermann, S. Antalic, W. Barth, M. Block, H.G. Burkhard *et al.*, Eur. Phys. J. A **48**, 62 (2012).
54. I. Muntian, S. Hofmann, Z. Patyk, A. Sobiczewski, Acta Phys. Pol. B, **34**, 2073 (2003) and A. Sobiczewski, private communication (2014).
55. I. Muntian, Z. Patyk, A. Sobiczewski, Phys. At. Nucl., **66**, 1015 (2003).
56. Yu.Ts. Oganessian, V.K. Utyonkov, Yu.V. Lobanov, F.Sh. Abdullin, A.N. Polyakov, I.V. Shirokovsky, Yu.S. Tsyganov, G.G. Gulbekian, S.L Bogomolov, B.N. Gikal *et al.*, Phys. Rev. **C69**, 054607 (2004).
57. Yu.Ts. Oganessian, J. Phys. G: Nucl. Part. Phys. **34**, R165 (2007).
58. A.G. Popeko, O.N. Malyshev, A.V. Yeremin, S. Hofmann, Nucl. Instrum. Methods Phys. Res. A **427**, 166 (1999).
59. R. Grzywacz, C.J. Gross, A. Korgul, S.N. Liddick, C. Mazzocchi, R.D. Page, K. Rykaczewski, Nucl. Instrum. Methods B **261**, 1103 (2007).
60. D. Miller, K. Miernik, D. Ackermann, R. Grzywacz, S. Heinz, F.P. Heßberger, S. Hofmann, K. Rykaczewski, H. Tan, *GSI Scientific Report 2011,* GSI Report **2012-1**, 220 (2012).
61. V. Zagrebaev, W. Greiner, Phys. Rev. C **78**, 034610 (2008).
62. R. Mann, D. Ackermann, S. Antalic, F.P. Heßberger, S. Hofmann, B. Kindler, P. Kuusiniemi, B. Lommel, K. Nishio, S. Saro *et al.*, *GSI Scientific Report 2005*, GSI Report **2006-1**, 198 (2006).
63. R.B. Firestone, S.Y.F. Chu, V.S. Shirley, C.M. Baglin, J. Zipkin, *Table of Isotopes CD-ROM*, Wiley-Interscience, 1996.
64. K.H. Schmidt, C.C. Sahm, K. Pielenz, H.G. Clerc, Z. Phys. A **316**, 19 (1984).
65. J.F. Ziegler, J.P. Biersack, M.D. Ziegler, *SRIM-2013.00, The Stopping and Range of Ions in Matter,* (2013) (http://www.SRIM.org).
66. V.K. Utyonkov, N.T. Brewer, Yu.Ts. Oganessian, K.P. Rykaczewski, F.Sh. Abdullin, S.N. Dmitriev, R.K. Grzywacz, M.G. Itkis, K. Miernik, A.N. Polyakov *et al.*, Phys. Rev. C **92**, 034609 (2015).
67. L. Stavsetra, K.E. Gregorich, J. Dvorak, P.A. Ellison, I. Dragojevic, M.A. Garcia, H. Nitsche, Phys. Rev. Lett. **103**, 132502 (2009).
68. Yu.Ts. Oganessian, V.K. Utyonkov, Yu.V. Lobanov, F.Sh. Abdullin, A.N. Polyakov, I.V. Shirokovsky, Yu.S. Tsyganov, G.G. Gulbekian, S.L Bogomolov, A.N. Mezentsev *et al.*, Phys. Rev. C **69**, 021601 (2004).

69. S. Hofmann, V. Ninov, F.P. Heßberger, P. Armbruster, H. Folger, G. Münzenberg, H.J. Schött, A.G. Popeko, A.V. Yeremin, A.N. Andreyev *et al.*, Z. Phys. A **350**, 281 (1995).
70. S. Hofmann, F.P. Heßberger, D. Ackermann, G. Münzenberg, S. Antalic, P. Cagarda, B. Kindler, J. Kojouharova, M. Leino, B. Lommel *et al.*, Eur. Phys. J. A, **14**, 147 (2002).
71. S. Hofmann, F.P. Heßberger, D. Ackermann, S. Antalic, P. Cagarda, S. Ćwiok, B. Kindler, J. Kojouharova, B. Lommel, R. Mann *et al.*, Eur. Phys. J. A **10**, 5 (2001).
72. S. Hofmann, V. Ninov, F.P. Heßberger, P. Armbruster, H. Folger, G. Münzenberg, H.J. Schött, A.G. Popeko, A.V. Yeremin, A.N. Andreyev *et al.*, Z. Phys. A **350**, 277 (1995).
73. J.H. Hamilton, S. Hofmann, Y.T. Oganessian, Annu. Rev. Nucl. Part. Sci. **63**, 383 (2013).
74. S. Hofmann, J. Phys. G: Nucl. Part. Phys. **42**, 114001 (2015).
75. S. Hofmann, D. Ackermann, S. Antalic, H.G. Burkhard, V.F. Comas, R. Dressler, Z. Gan, S. Heinz, J.A. Heredia, F.P. Heßberger *et al.,* Eur. Phys. J. A **32**, 251 (2007).
76. P.A. Ellison, K.E. Gregorich, J.S. Berryman, D.L. Bleuel, R.M. Clark, I. Dragojevic, J. Dvorak, P. Fallon, C. Fineman-Sotomayor, J.M. Gates *et al.*, Phys. Rev. Lett. **105**, 182701 (2010).
77. J.M. Gates, Ch.E. Düllmann, M. Schädel, A. Yakushev, A. Türler, K. Eberhardt, J.V. Kratz, D. Ackermann, L.-L. Andersson, M. Block *et al.*, Phys. Rev. C **83**, 054618 (2011).
78. Yu.Ts. Oganessian, F.Sh. Abdullin, C. Alexander, J. Binder, R.A. Boll, S.N. Dmitriev, J. Ezold, K. Felker, J.M. Gostic, R.K. Grzywacz *et al.*, Phys. Rev. Lett. **109**, 162501 (2012).
79. Yu.Ts. Oganessian, V.K. Utyonkov, Yu.V. Lobanov, F.Sh. Abdullin, A.N. Polyakov, I.V. Shirokovsky, Yu.S. Tsyganov, G.G. Gulbekian, S.L. Bogomolov, B.N. Gikal *et al.*, Phys. Rev. C **62**, 041604 (2000).
80. Yu.Ts. Oganessian, V.K. Utyonkov, Yu.V. Lobanov, F.Sh. Abdullin, A.N. Polyakov, I.V. Shirokovsky, Yu.S. Tsyganov, G.G. Gulbekian, S.L. Bogomolov, B.N. Gikal *et al.*, Phys. Rev. C **63**, 011301 (2000).
81. Yu.Ts. Oganessian, V.K. Utyonkov, K.J. Moody, Phys. Atom. Nucl. **64**, 1349 (2001).
82. Yu.Ts. Oganessian, V.K. Utyonkov, Yu.V. Lobanov, F.Sh. Abdullin, A.N. Polyakov, I.V. Shirokovsky, Yu.S. Tsyganov, G.G. Gulbekian, S.L Bogomolov, B.N. Gikal *et al.*, Preprint JINR E7-2002-287 (2002).
83. Yu.Ts. Oganessian, V.K. Utyonkov, Yu.V. Lobanov, F.Sh. Abdullin, A.N. Polyakov, I.V. Shirokovsky, Yu.S. Tsyganov, G.G. Gulbekian, S.L Bogomolov, B.N. Gikal, *et al.*, Phys. Rev. C **70**, 064609 (2004).
84. Yu.Ts. Oganessian, V.K. Utyonkov, Yu.V. Lobanov, F.Sh. Abdullin, A.N. Polyakov, I.V. Shirokovsky, Yu.S. Tsyganov, G.G. Gulbekian, S.L. Bogomolov, B.N. Gikal *et al.*, *JINR preprint* **E7-2004-160**, pp. 1–28 (2004), (http://www.jinr.ru/publish/Preprints/2004/160(E7-2004-160).pdf).
85. Yu.Ts. Oganessian, V.K. Utyonkov, Yu.V. Lobanov, F.Sh. Abdullin, A.N. Polyakov, R.N. Sagaidak, I.V. Shirokovsky, Yu.S. Tsyganov, A.A. Voinov, G.G. Gulbekian, *et al.*, Phys. Rev. C **74**, 044602 (2006).
86. Yu.Ts. Oganessian, A.V. Yeremin, A.G. Popeko, O.N. Malyshev, A.V. Belozerov, G.V. Buklanov, M.L. Chelnokov, V.I. Chepigin, V.A. Gorshkov, S. Hofmann *et al.*, Nucl. Phys. A **734**, 196 (2004).
87. Yu.Ts. Oganessian, A.V. Yeremin, G.G. Gulbekian, S.L. Bogomolov, V.I. Chepigin, B.N. Gikal, V.A. Gorshkov, M.G. Itkis, A.P. Kabachenko, V.B. Kutner *et al.*, Eur. Phys. J. A **5**, 63 (1999).
88. Yu.Ts. Oganessian, A.V. Yeremin, V.I. Chepigin, M.G. Itkis, A.P. Kabachenko, O. Konstantinesky, M. Konstantinesky, O.N. Malyshev, A.G. Popeko, J. Roháĉ *et al.*, Eur. Phys. J. A **5**, 63 (1999).
89. Yu.Ts. Oganessian, A.V. Yeremin, A.G. Popeko, S.L. Bogomolov, G.V. Buklanov, M.L. Chelnokov, V.I. Chepigin, B.N. Gikal, V.A. Gorshkov, G.G. Gulbekian *et al.*, Nature **400**, 242 (1999).
90. R. Smolanczuk, Phys. Rev. C **56**, 812 (1997).
91. M. Wang, G. Audi, A.H. Wapstra, F.G. Kondev, M. MacCormick, X. Xu, B. Pfeiffer, Chinese Phys. **36**, 1603 (2012).
92. K.H. Schmidt, Eur. Phys. J. A **8**, 141 (2000).
93. I. Muntian, Z. Patyk, A. Sobiczewski, Acta Phys. Pol. B **32**, 691 (2001).
94. A. Sobiczewski, Acta Phys. Pol. **42**, 1871 (2011).
95. J.O. Rasmussen, Phys. Rev. **113**, 1593 (1959).
96. G. Igo, Phys. Rev. **115**, 1665 (1959).
97. P. Möller, J.R. Nix, W.D. Myers, W.J. Świątecki, At. Data Nucl. Data Tables **59**, 185 (1995).
98. Yu.Ts. Oganessian, V.K. Utyonkov, F.Sh. Abdullin, S.N. Dmitriev, R. Graeger, R.A. Henderson, M.G. Itkis, Yu.V. Lobanov, A.N. Mezentsev, K.J. Moody *et al.*, Phys. Rev. C **87**, 034605 (2013).
99. S. Liran, A. Marinov, N. Zeldes, Phys. Rev. C, **63**, 017302 (2000), arXiv:nucl-th/0102055.
100. S. Ćwiok, W. Nazarewicz, P.H. Heenen, Phys. Rev. Lett. **83**, 1108 (1999).
101. S. Cwiok, S. Hofmann, W. Nazarewicz, Nucl. Phys. A **573**, 356 (1994).
102. V.I. Zagrebaev, A.V. Karpov, W. Greiner, Phys. Rev. C, **85**, 014608 (2012).
103. S. Hofmann, P. Armbruster, G. Berthes, T. Faestermann, A. Gillitzer, F.P. Heßberger, W. Kurcewicz, G. Münzenberg, K. Poppensieker, H.J. Schött, I. Zychor, Z. Phys. A **333**, 107 (1989).
104. S. Ćwiok, P.H. Heenen, W. Nazarewicz, Nature **433**, 705 (2005).
105. P. Jachimowicz, M. Kowal, J. Skalski, Phys. Rev C **83**, 054302 (2011).
106. K. Siwek-Wilczyńska, T. Cap, J. Wilczyński, Int. J. Mod. Phys. E **19**, 500 (2010).
107. A.K. Nasirov, G. Giardina, G. Mandaglio, M. Manganaro, F. Hanappe, S. Heinz, S. Hofmann, A.I. Muminov, W. Scheid, Phys. Rev. C **79**, 024606 (2009).
108. G.G. Adamian, N.V. Antonenko, W. Scheid, Eur. Phys. J. A **41**, 235 (2009).
109. K. Siwek-Wilczyńska, T. Cap, M. Kowal, A. Sobiczewski, J. Wilczyński, Phys. Rev. C **86**, 014611 (2012).
110. T. Cap, K. Siwek-Wilczyńska, M. Kowal, J. Wilczyński, Phys. Rev. C **88**, 037603 (2013).
111. J.C. Pei, W. Nazarewicz, J.A. Sheikh, A.K. Kerman, Phys. Rev. Lett., **102**, 192501 (2009).
112. J.A. Sheikh, W. Nazarewicz, J.C. Pei, Phys. Rev. C, **80**,011302 (2009).

113. A.N. Bezbakh, T.M. Shneidman, G.G. Adamian, N.V. Antonenko, J. Phys. Conf. Ser. **580**, 012026 (2015).
114. I. Muntian, Z. Patyk, A. Sobiczewski, Acta Phys. Pol. B **34**, 2141 (2003).
115. M.G. Itkis, Yu. Ts. Oganessian, V.I. Zagrebaev, Phys. Rev. C **65**, 044602 (2002).
116. V.I. Zagrebaev, M.G. Itkis, Yu.Ts. Oganessian, Phys. At. Nucl. **66**, 1033 (2003).
117. G. Henning, T.L. Khoo, A. Lopez-Martens, D. Seweryniak, M. Alcorta, M. Asai, B.B. Back, P.F. Bertone, D. Boilley, M.P. Carpenter *et al.*, Phys. Rev. Lett. **113**, 262505 (2014).
118. M. Kowal, P. Jachimowicz, A. Sobiczewski, Phys. Rev. C **82**, 014303 (2010) and A. Sobiczewski, private communication (2014).
119. P. Möller, A.J. Sierk, T. Ichikawa, A. Iwamoto, M. Mumpower, Phys. Rev. C, **91**, 024310 (2015).
120. S. Hofmann, S. Heinz, R. Mann, J. Maurer, G. Münzenberg, S. Antalic, W. Barth, L. Dahl, K. Eberhardt, R. Grzywacz *et al.*, Eur. Phys. J. A, submitted (2015).
121. G. Audi, M. Wang, A.H. Wapstra, F.G. Kondev, M. MacCormick, X. Xu, B. Pfeiffer, Chinese Phys. **36**, 1287 (2012).
122. W.J. Świątecki, K. Siwek-Wilczyńska, J. Wilczyński Acta Phys. Pol. B **38**, 1565 (2007).
123. R. Bass, Nucl. Phys. A **231**, 45 (1974).
124. P. Möller, A.J. Sierk, T. Ichikawa, A. Iwamoto, R. Bengtsson, H. Uhrenholt, S. Åberg, Phys. Rev. C **79**, 064304 (2009).
125. S. Heinz, V. Comas, S. Hofmann, D. Ackermann, J. Heredia, F.P. Heßberger, J. Khuyagbaatar, B. Kindler, B. Lommel, R. Mann, Eur. Phys. J. A **43**, 181 (2010).
126. H.M. Devaraja, S. Heinz, O. Beliuskina, V. Comas, S. Hofmann, C. Hornung, G. Münzenberg, K. Nishio, D. Ackermann, Y.K. Gambhir *et al.*, Phys. Lett. B **748**, 199 (2015).
127. V.K. Utyonkov, *Int. Symposium 'Super Heavy Nuclei', College Station, Texas, USA* http://cyclotron.tamu.edu/she2015/assets/pdfs/presentations/Utyonkov_SHE_2015_TAMU.pdf, 2015.
128. K. Morita, *et al.*, *RIKEN Accelerator Progress Report (APR)* to be published, 2015.
129. K. Morita, *SHE research at RIKEN/GARIS, Int. Symposium 'Super Heavy Nuclei', College Station, Texas, USA*, http://cyclotron.tamu.edu/she2015/assets/pdfs/presentations/Morita_SHE_2015_TAMU.pdf, 2015.
130. V.I. Zagrebaev, Yu.Ts. Oganessian, M.G. Itkis, W. Greiner, Phys. Rev. C **73**, 31602(R) (2006).
131. S. Heinz, V. Comas, F.P. Heßberger, S. Hofmann, D. Ackermann, H.G. Burkhard, Z. Gan, J. Heredia, J. Khuyagbaatar, B. Kindler *et al.*, Eur. Phys. J. A **38**, 227 (2008).
132. W.J. Świątecki, K. Siwek-Wilczyńska, J. Wilczyński, Phys. Rev. C *71*, 014602 (2005).
133. C.Y. Wong, Ann. Phys. **77**, 279 (1973).
134. K. Dietrich and K. Pomorski, Phys. Rev. Lett. **80**, 37 (1998).
135. S. Hofmann, *SHIP-2000 - A proposal for the study of superheavy elements*, GSI-Report **99-02**, pp. 1−16 (1999).
136. S. Hofmann, D. Ackermann, W. Barth, L. Dahl, F.P. Heßberger, B. Kindler, B. Lommel, R. Mann, G. Münzenberg, K. Tinschert, U. Ratzinger, A. Schempp, *International Symposium on Exotic Nuclei, EXON-2004* (World Scientific Publishing, Singapore) 2005.
137. W. Barth, *Int. Symposium 'Super Heavy Nuclei', College Station, Texas, USA* http://cyclotron.tamu.edu/she2015/assets/pdfs/presentations/Barth_SHE_2015_TAMU.pdf, 2015.